Summer 8-20-2019

Texture-based Deep Neural Network for Histopathology Cancer Whole Slide Image (WSI) Classification

NELSON Zange TSAKU

Texture-based Deep Neural Network for Histopathology Cancer Whole Slide Image (WSI) Classification

A Thesis Presented to

The Faculty of the Computer Science Department

By

NELSON ZANGE TSAKU

In Partial Fulfillment

of the Requirements for the Degree of

Master of Science, Computer Science

Kennesaw State University

July 2018

Texture-based Deep Neural Network for Histopathology Cancer Whole Slide Image (WSI) Classification

Approved:

_____

Dr. Mingon Kang - Advisor

_____

Dr. Dan Chia-Tien Lo– Department Chair

_____

Dr. Jon Preston - Dean

In presenting this thesis as a partial fulfillment of the requirements for an advanced degree from Kennesaw State University, I agree that the university library shall make it available for inspection and circulation in accordance with its regulations governing materials of this type. I agree that permission to copy from, or to publish, this thesis may be granted by the professor under whose direction it was written, or, in his absence, by the dean of the appropriate school when such copying or publication is solely for scholarly purposes and does not involve potential financial gain. It is understood that any copying from or publication of, this thesis which involves potential financial gain will not be allowed without written permission.

_____

Nelson Zange Tsaku

Notice To Borrowers

Unpublished theses deposited in the Library of Kennesaw State University must be used only in accordance with the stipulations prescribed by the author in the preceding statement.

The author of this thesis is:

Nelson Zange Tsaku

S Marietta PKWY,

Marietta, GA 30060

The director of this thesis is:

Dr. Mingon Kang

1100 S Marietta PKWY,

Marietta, GA 30060

Users of this thesis not regularly enrolled as students at Kennesaw State University are required to attest acceptance of the preceding stipulations by signing below. Libraries borrowing this thesis for the use of their patrons are required to see that each user records here the information requested.

To my Parents and my siblings

ACKNOWLEDGEMENTS

With all respect, I would first like to thank God for giving me knowledge, strength and support I need. Second, I would like to express my appreciation to my advisor, Dr. Mingon Kang, for his valuable guidance, support and constant encouragement throughout this entire research. Last, I would like to express my gratitude to my beloved parents, brothers and sister, and other family members for the motivation, inspiration and moral support.

ABSTRACT

Automatic histopathological Whole Slide Image (WSI) analysis for cancer classification has been highlighted along with the advancements in microscopic imaging techniques. However, manual examination and diagnosis with WSIs is time-consuming and tiresome. Recently, deep convolutional neural networks have succeeded in histopathological image analysis. In this paper, we propose a novel cancer texture-based deep neural network (CAT-Net) that learns scalable texture features from histopathological WSIs. The innovation of CAT-Net is twofold: (1) capturing invariant spatial patterns by dilated convolutional layers and (2) Reducing model complexity while improving performance. Moreover, CAT-Net can provide discriminative texture patterns formed on cancerous regions of histopathological images compared to normal regions. The proposed method outperformed the current state-of-the-art benchmark methods on accuracy, precision, recall, and F1 score.

Table of Contents

LIST OF TABLES

LIST OF FIGURES

CHAPTER 1

INTRODUCTION

1.1 Histopathology

In clinical medicine, histopathology refers to the examination of a biopsy or surgical specimen by a pathologist, after the specimen has been processed and histological sections have been placed onto glass slides. The much broader branch, known as Histochemistry is concerned with the identification and distribution of the chemical constituents of tissues by means of stains, indicators, and microscopy. During the process, when antibodies bind to antigen in the tissue sample, an enzyme or dye is activated, and the antigen can then be seen under a microscope. The latter is called Immunohistochemistry, and it is used to help diagnose diseases such as Cancer. It may also be used to identify the difference between different types of cancer. Immunohistochemistry comprises two phases: (1) slides preparation and stages involved for the reaction; (2) interpretation and quantification of the obtained expression. Immunohistochemistry is an important tool for scientific research and also a complementary technique for the elucidation of differential diagnoses which are not determinable by conventional analysis with hematoxylin and eosin (H&E) or Cytokeratins (CK).

1.2 Carcinoma Cancer

Carcinoma is a type of cancer that starts in cells that make up the skin or the tissue lining organs, such as the liver or kidneys. Like other types of cancer, carcinomas are abnormal cells that divide without control. They are able to spread to other parts of the body, but do not always. "Carcinoma in situ" stays in the cells where it started.

1.2.1 Types of Carcinoma Cancer

Depending on the body part where the cancer spreads to, there are five common types of carcinoma: Basal cell carcinoma, Squamous cell carcinoma, renal cell carcinoma, and Ductal carcinoma in situ (DCIS), Invasive ductal carcinoma and Adenocarcinoma. In this report, we focus on Adenocarcinoma.

1.2.2 Adenocarcinoma

Adenocarcinoma starts in cells called "glandular cells." These cells make mucus and other fluids. The glandular cells are found in different organs in our body. Adenocarcinomas can occur in different parts of the body. Some examples of cancers that can be adenocarcinomas include lung, pancreatic, and colorectal types.

1.2.3 Biological Data Origin

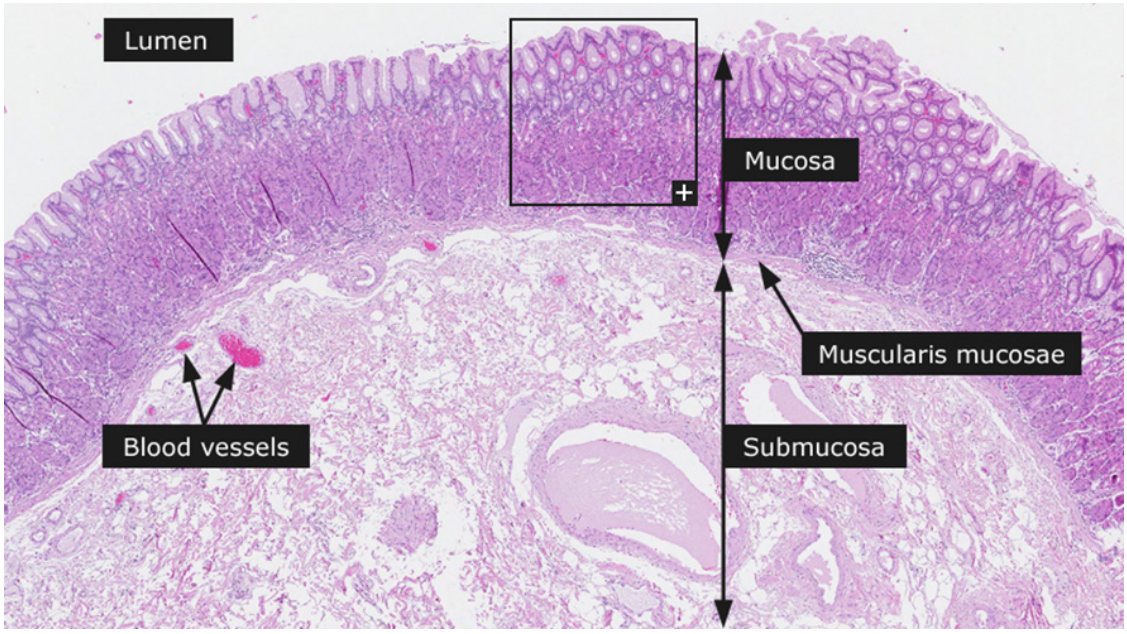

Figure 1: Normal tissues in the stomach region where cancer is developed

Most biopsy in the data were obtained from mucosa, where cancer is developed. *Figure 1* shows a normal tissue in stomach. Mucosa consists of glands of epithelial cell. When zooming in the rectangle in the above figure, normal glands are clearly shown.

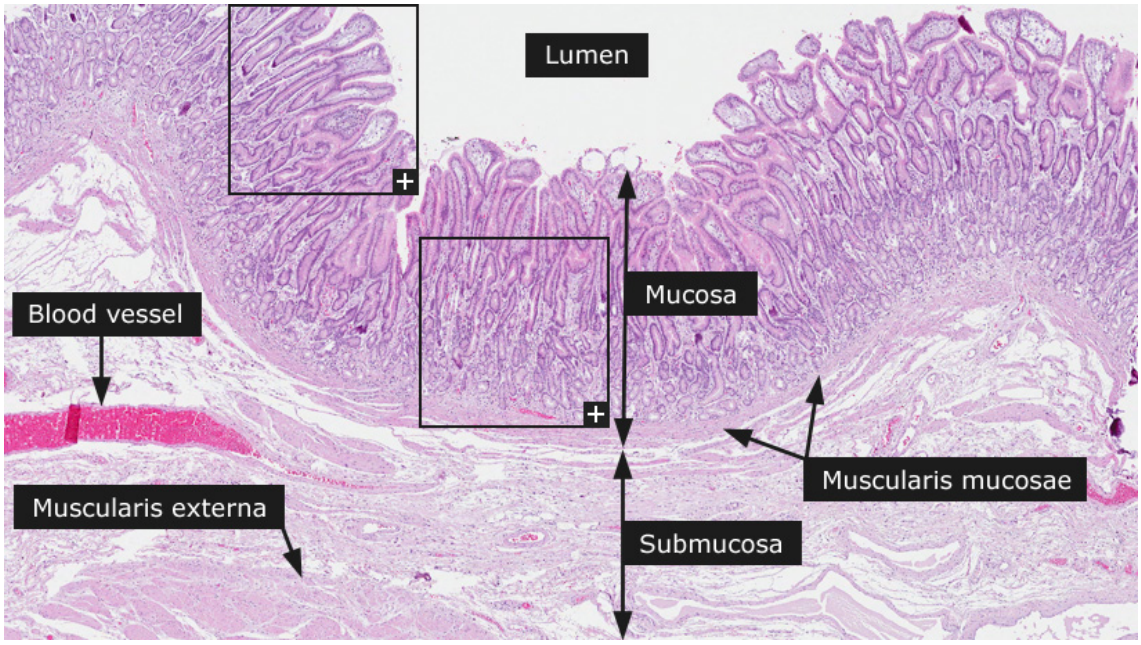

Figure 2: Epithelial cells forming glands

Figure 2 shows epithelial cells (glandular cells) that forms glands, and these cells becomes cancer in a certain condition. There are several types of cancers on stomach, but our data is specialized on adenocarcinoma (the origin of “adeno” which means “glands”), which are originates from epithelial (glandular) cells.

The data collected consists of two main stains: Haematoxylin and eosin stain (HE stain), which is one of the principal tissue stains used in histology; and Cytokeratins Stain (CK stain), an immunohistochemical marker that has similar functionality as HE, and can check whether the carcinoma is originated from epithelial cells or not.

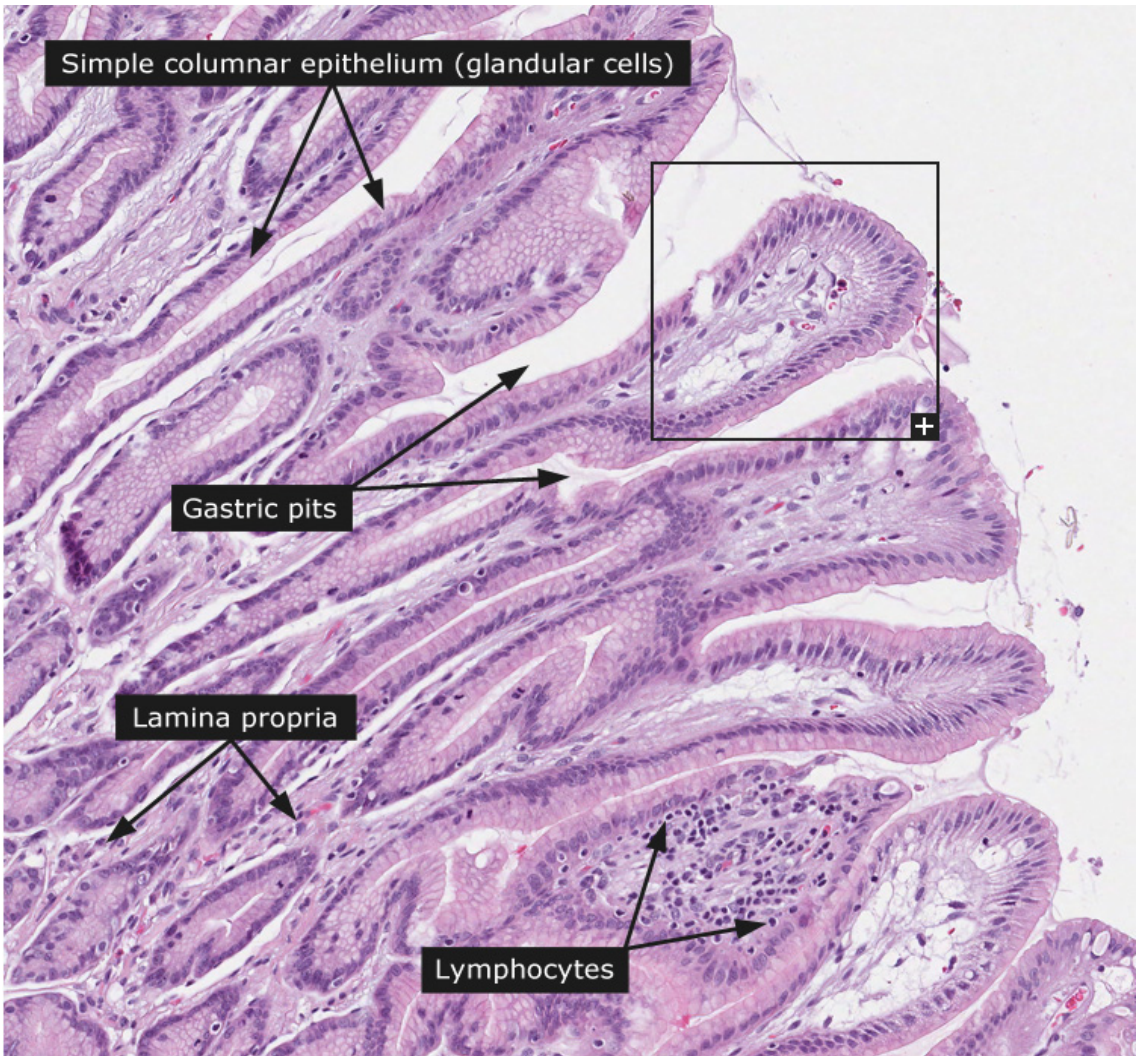

Figure 3: Gastric pits and simple columnar glandular cells

If we zoom into the rectangular box in *Figure 3*, we can look at epithelial cells more clearly annotated by “glandular cells” in *Figure 4*. A circular component dyed in purple is nucleus, and the parts that surrounds the nucleus (in pink) are cytoplasm. The cancer originated from the cells is carcinoma. The cancer cells proliferate rapidly, and they invade into lamina propria (belong to mucosa). Then, they invade into deeper layer of submucosa and musclaris externa.

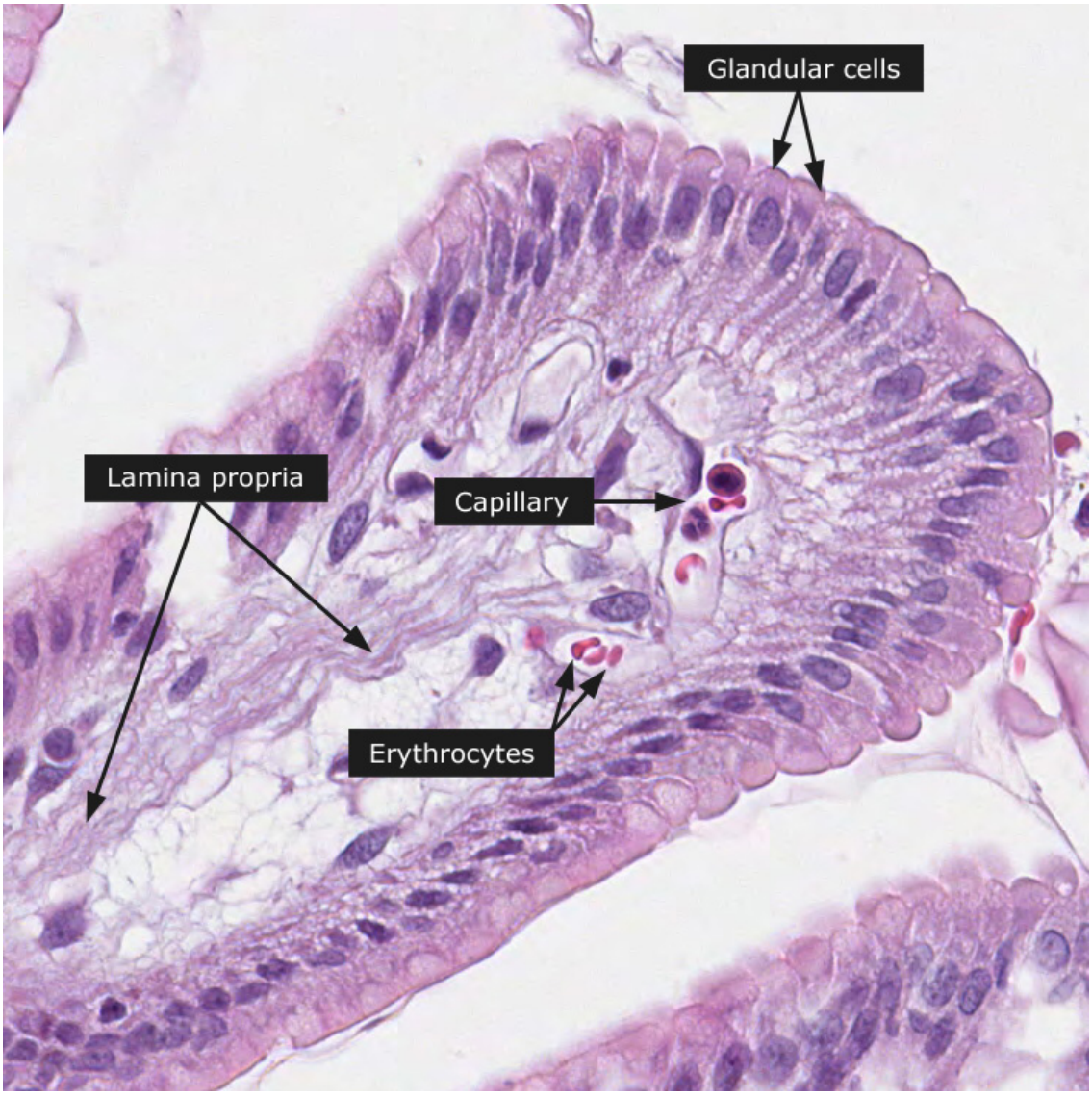

Figure 4: Focused parts of the glandular cells: lamina propria, capillary, Erthrocytes

Among carcinoma, cancer that has similar shapes with normal glands is called “adenocarcinoma”, and they are the most common cancer.

Our collected data is categorized the data into four: (1) well-differentiated, moderately-differentiated, poorly-differentiated, and poorly cohesive carcinoma. The first three categories are based on the differentiation of adenocarcinoma, i.e. how well the tissues form glands. These differences cause patients’ prognosis. For example, if the differentiation is not good like “poorly differentiated”, the survival time would be very short.

In the last category, “poorly cohesive”, carcinoma’s shape is not common and the differentiation is not extremely poor, so the carcinoma tend to invade separately and the patients’ survival rate is very low. Furthermore, pathologist often miss the carcinoma. And, it is often not easy to detect them by HE Immunohistochemistry, so additional analysis is done with CK Immunohistochemistry to clearly recognize them.

The reason why the data is categorized into four is that (1) these are very common cases that pathologists commonly observe and (2) the performance of deep learning may produce different results depending on the categories, which will be useful in analysis. Table 1 below clear outlines the different categories.

Category	Image Sample
Well-differentiated	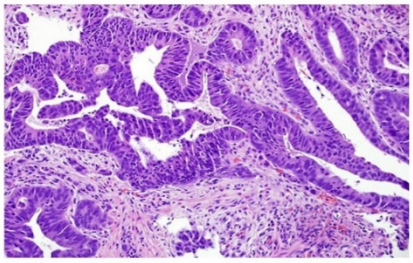 Well–differentiated forms glands very effectively
Moderately-differentiated	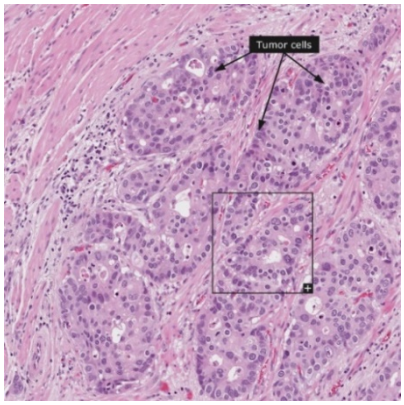 In moderately – differentiated, glands are fusioned each other.
Poorly-differentiated	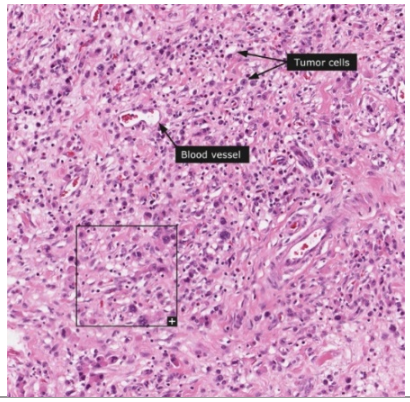 In poorly – differentiated, the shape of glands are not well observed.
Poorly-cohesive	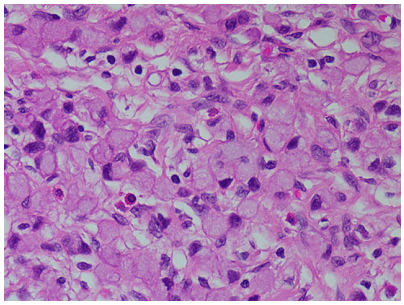 In poorly cohesive, cells, where nucleus is pushed out to next so shaped as “crescent moon” and cytoplasm looks blurry, are carcinoma. There are many additional carcinoma in this figure near by the annotation. It is also called “signet-ring cell feature”.

Table 1: Different categories of collected data and description

1.3 Diagnosis

Diagnostic tests vary according to where the cancer is located. When diagnosing adenocarcinoma, the following tests may be performed:

Biopsy: Removing a sample of abnormal tissue in the body. A pathologist examines the tissue under a microscope to determine whether cancer is present. If it is, a biopsy may be used to determine whether the cancer originated at the biopsied site or in another part of the body.

Computed tomography (CT) scan: This is an X-ray procedure using a computer to take detailed, three-dimensional pictures of abnormal tissue in the body. CT scans are also performed during treatment to see whether the cancer is responding to treatment.

Magnetic resonance imaging (MRI): MRIs use radiofrequency waves to create detailed cross-sectional images of different parts of the body.

1.4 Treatment

Treatment for adenocarcinoma varies depending on where it grows in the body, it may include:

Surgery: Adenocarcinoma is often treated by surgically removing cancerous glandular tissue, as well as some surrounding tissue. Minimally invasive surgical methods may help reduce healing time and reduce the risk of infection after surgery.

Radiation therapy: This adenocarcinoma treatment option is typically used in combination with surgery and/or chemotherapy. Advanced radiation therapies use image guidance

before and during treatment to target adenocarcinoma tumors as part of a process designed to spare healthy tissues and surrounding organs.

Chemotherapy: Chemotherapy treats adenocarcinoma with drugs designed to destroy cancer cells, either throughout the whole body or in a specific area. In some cases, chemotherapy may be used in combination with other treatments, such as radiation therapy or surgery.

1.5 Problems & Challenges Digital Pathology diagnosis

1.5.1 Digital Pathology

Gastric Carcinoma is the second leading cause of cancer-associated deaths in the world, responsible for 738,000 deaths annually. Pathologists, medical specialty consist of histologically analyzing the structure and elements of gastric cancer tissue images.

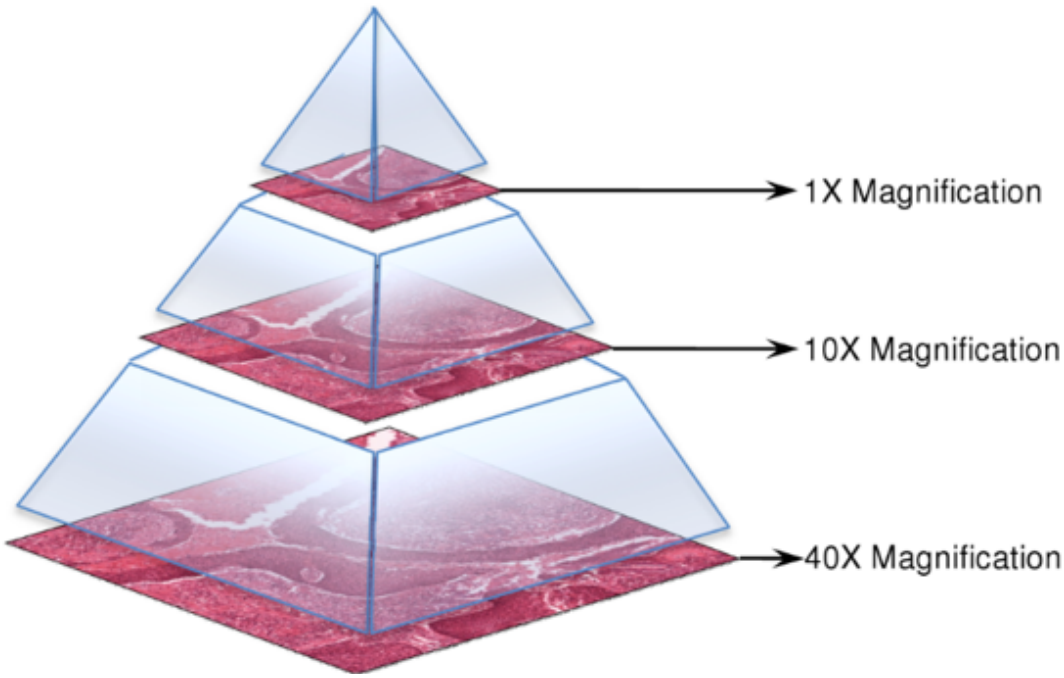

Figure 5: Multi-resolution Whole Slide Image [1]

Pathologists visually examine and diagnose macroscopic tissue images to identify and analyze abnormalities.

The recent advents in computing pathology also made it possible to predict survival of a cancer patient [1, 2]. It is very important that the field of precision medicine make constant advances. This is to ensure an accurate diagnosis of the cancer that the patient is suffering from. It is important that there be standardized, accurate and reproducible pathological diagnoses for advancing precision medicine. As stated by [3], if we look back in the past, the microscope was the primary tool used by pathologists, ever since the mid-19th century. The images formed by these microscopes had many limitations after qualitative visual analysis of them, which included lack of standardization, diagnostic errors and the significant cognitive load required to manually evaluate millions of cells across hundreds of slides. To manually conduct a pathological review of the epithelial cells from sample images as in *Figure 4* is time consuming and laborious, especially in cases where cells are poorly differentiated. To improve accuracy of adenocarcinoma detection, many clinical laboratories have tried applying proteins such as immunohistochemistry [4] for HE/CK [5] on carcinoma cancer cells; however, this task is time-consuming, error-prone, and subjective, causing intra- and inter- observer variability among pathologists [3].

1.5.2 Computational Challenges

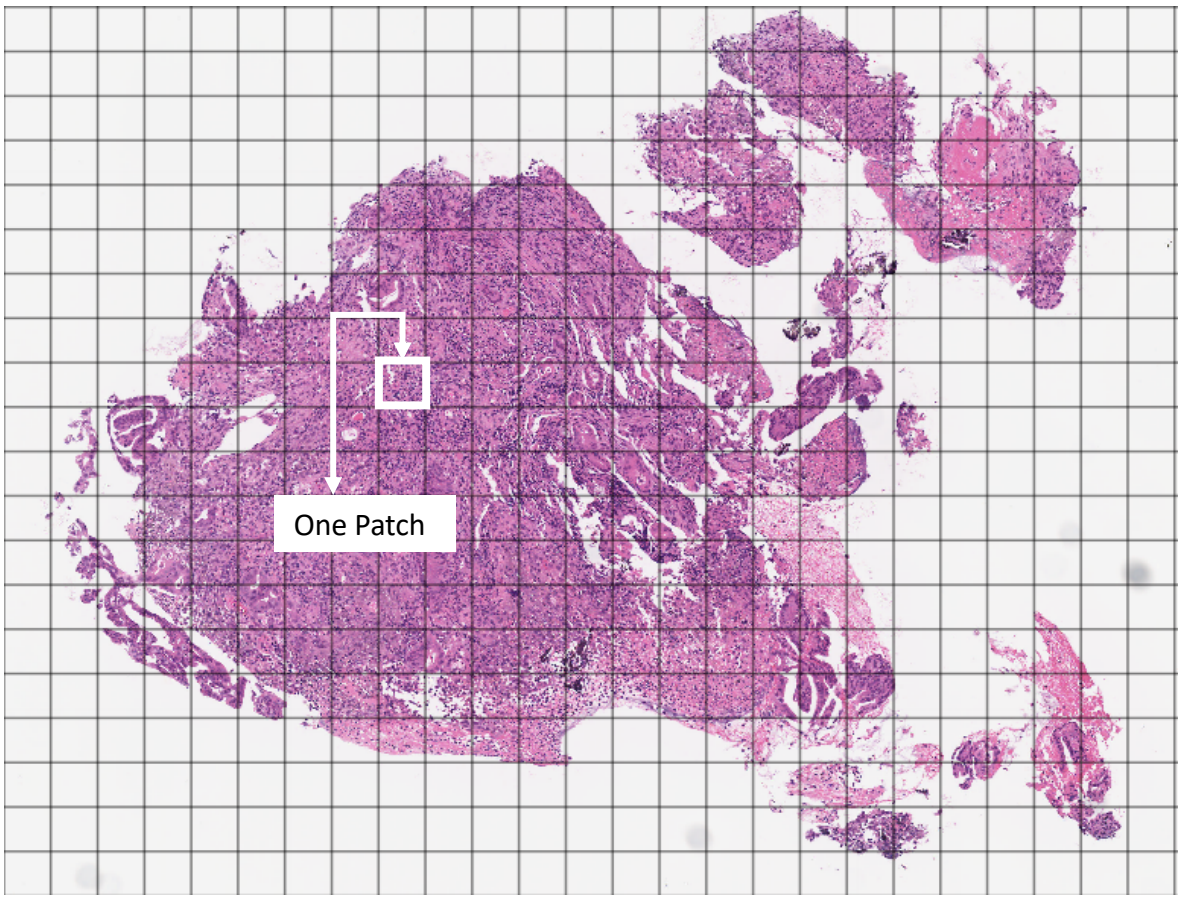

Figure 6: Patching is generally used to represent larger scans. For instance, every patch could be a 256 by 256 pixel image at x40

Over the several decades there has been an interest in developing computer software to assist in the analysis of digital microscopic images in pathology. Therefore, computer-assisted image analysis systems have been developed to aid in the detection of epithelial tissues from digital slides of sentinel lymph nodes; however, clinically, these systems are not used due to the lack of standardization of image formats, system noise, and lack of clinical and technical studies on digital pathology systems [6]. Hence, active research is currently taking place to develop effective and cost efficient methods for

sentinel lymph node evaluation, as there is a heavy requirement for a high-performing system that could increase accuracy and reduce cognitive load at low cost.

WSI deals with gigapixel digital images of extremely large dimensions. Image sizes larger than ~10^6 by ~10^6 pixels are quite common. Deep CNNs, however, operate on much smaller image dimensions (i.e., not larger than 350 by 350 pixels). Dividing an image into various small tiles, (known as "Patching" as in *Figure 6*) is a potential solution for not just AI algorithms but also for general computer vision methods. However, even for patches, one generally needs to down sample them in order to be able to feed them into a deep network. A region smaller than 1.5 µm2 may not be suitable for many diagnostic purposes and this is, most of the time, at least 1000 by 1000 pixels. Down sampling these patches may result in loss of crucial information. On the other hand, deep nets with larger input sizes would need much deeper topology and much larger number of neurons making them even more difficult and perhaps impossible to train. Of note, patch-based ANNs have been shown to outperform image-based ANNs [7].

1.6 Goal of Thesis

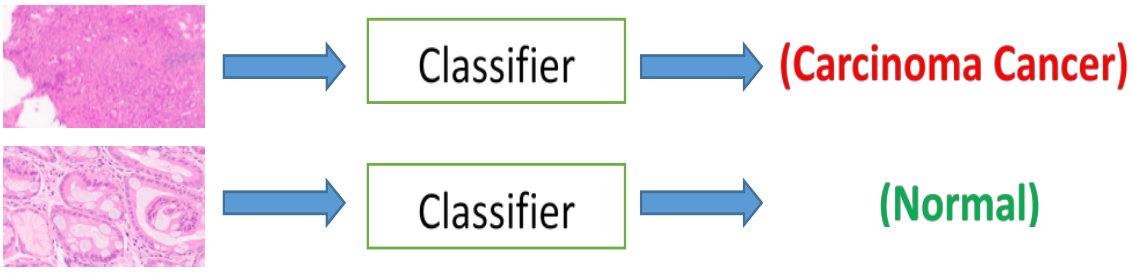

Figure 7: Patch classification pipeline

The goal of this thesis is develop a deep learning classification pipeline for detection of carcinoma cancer from whole slide images of stomach epithelial lymph node. The classification pipeline consists of four stages:

1. Whole slide Image (WSI) preprocessing
2. Train Cancer Texture (CAT-Net) model for tile-based classification
3. Build tumor probability heat map with test scores from trained model
4. Post-processing on heat maps for slide based classification

Traditional computer aided methods are not useful for clinical practices because they require pathologist to set several manual parameters to obtain accurate results; hence the task is time-consuming, error-prone, and subjective, causing intra- and inter- observer variability among pathologists.

The key aspect of this thesis is to develop a proposed method that will prove to be highly useful and can be easily operated in clinical settings with minimal human intervention. The effectiveness of the proposed system is evaluated by performing extensive experiments on real life gastroscopic biopsy specimen of 94 cases at the Gyeongsang National University Changwon Hospital (Changwon, Korea) collected between February 2016 and July 2017, stained with hematoxylin and eosin (H&E) using standard protocols in routine clinical care. Figure 7 shows the proposed patch-based whole slide image classification system for identifying carcinoma cancer.

CHAPTER 2: RELATED WORKS

2.1 Related works

Computational techniques to gastric tissue image analysis is a potential challenge in digital histopathology. In related works, much research from traditional image processing approaches to deep learning algorithms have been studied and developed for quantifying histopathology images. For instance, to classify suspicious regions for gastric cancer, a computer-based pathology system was proposed, which used histological analysis of hematoxylin and eosin (H & E)-stained sections [8]. This computational system mainly consists of an Info-Max algorithm and a support vector machine classifier to detect suspicious cancer regions and classify them respectively. More so, a semi-supervised Multi Instance Learning (MIL) tissue classifier was leveraged [9], to detect gastric cancer in H & E stained section tissue images. Later on, high-quality features based on color, texture, and morphology of nuclei, were extracted from nuclei segmentation approaches, which played an important role in segmentation of digital pathology images for cancer research. From the later, high quality features are extracted by applying a minimum-model nuclei segmentation method, and subsequently used as input of an AdaBoost classifier for classification of gastric cancer. Later on, a graph-based method for gastric cancer classification was proposed, which rigorously utilize cell nuclei morphology as vertex attributes, and neighborhood information as edge attributes [10]. The method involves H & E stained whole slide image analysis and Adaboost classification. These classical methods

mostly used three image analysis based methods: color normalization, nuclear segmentation and feature extraction.

2.2 Image analysis based methods

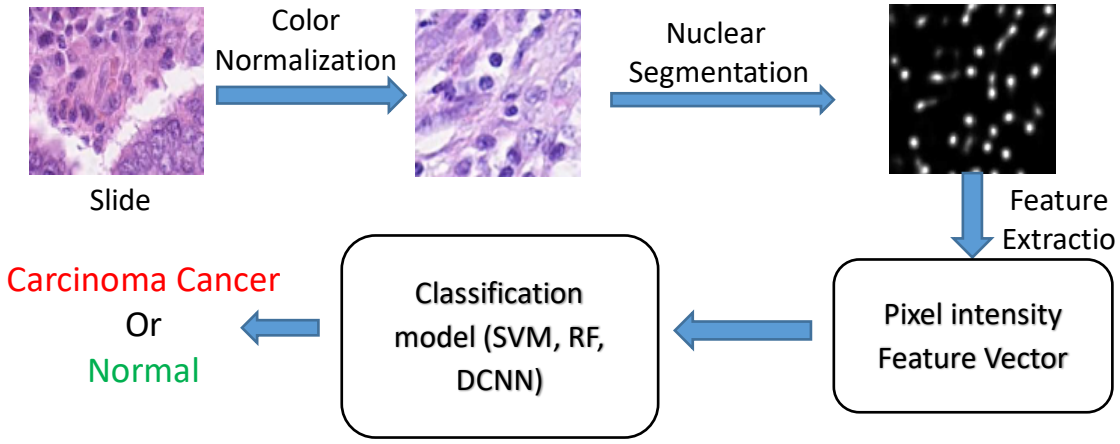

Figure 8: Classical method architecture

Decades ago, there have been an interest of scientists to develop computer aided methods for identifying carcinoma cancer from GigaPixel (~10^6 x ~10^6 pixels) histological images. These historical methods are mainly focused on low level image analysis [11] tasks such as color normalization, nuclear segmentation, and feature extraction [12, 13]. Detailed architecture of these methods is illustrated in *Figure 8*. In this section, we will explain each stage of the classical method in detail.

2.2.1 Color normalization

Color normalization is a topic in computer vision concerned with artificial color vision and object recognition. The technique is used for reducing the difference between different tissue samples, introduced due to applied staining and various scanning conditions during preparation of whole slide images [14]. With staining, it becomes easier to analyze images as it helps to highlight structural elements into whole slide images. According to [13], there are multiples ways in which staining can be applied. One method is to calibrate targets or finding pixel intensity patterns from multiple images and then fit polynomial surface over source images. Another highly used method in industry is to match histograms of different source images. [13] Also mentioned that, approach based on gradient calculation from LUV color space proved reliable for highlighting tissue structures from WSI images. As color normalization helps in building generalized solution, it is considered to be the most important step for building histological image analysis technique. *Figure 8* illustrates an example of Color Normalization operation on digital WSI.

2.2.2 Nuclear Segmentation

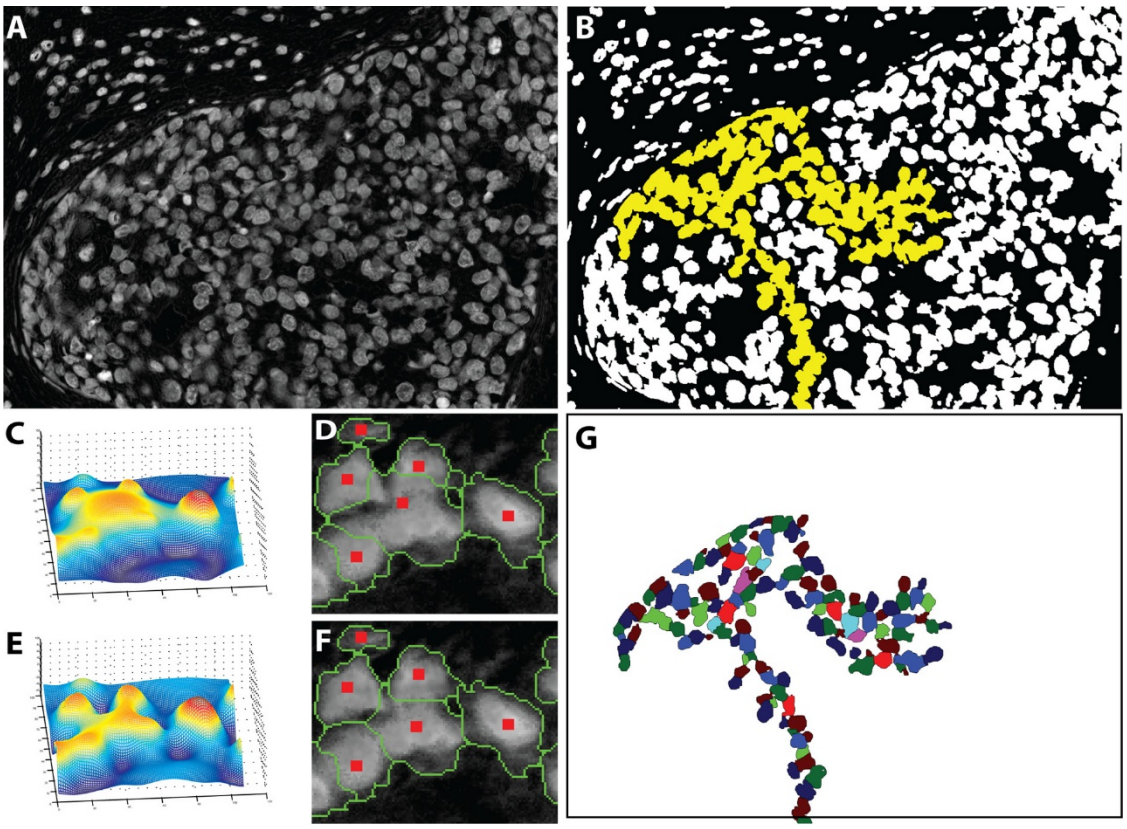

Figure 9: Illustrating key steps of the proposed nuclear segmentation method. (A) Nuclear channel from spectral unmixing. (B) Foreground extraction results. Pixels marked yellow represent a large connected component. (C) Surface plot of the multiscale LoG filtering results for a small region. (D) Initial segmentation based on the LoG. (E) Surface plot of the distance-map-constrained multiscale LoG. (F) Improved initial segmentation resulting from the distance-constrained LoG. (G) Color coding of the yellow pixels in panel (B). [22] (From C. Szegedy et al.)

Nuclear segmentation in digital microscopic tissue images can enable extraction of high quality features for nuclear morphometric and other analyses in computational pathology. This step follows directly after color normalization. It is the process of identifying nuclei structure present in whole slide images [15]. This is commonly a first step to counting cells, quantifying molecular markers (antigens) of interest in healthy and

pathologic specimens, and also for quantifying aspects of normal/diseased tissue architecture [13]. Moreover, these properties also allows to determine sub-types of detected cells which helps pathologist to determine specific type of cancer disease patient is suffering from. For example, the presence of large number of malignant cells in a carcinoma cancer histological image is a clear indication of a higher cancer stage. As per [13], other significant measure to decide severity of disease is to count nuclei based on texture from histological images, as a higher count is a strong indication of poor disease outcome for some cancer situations. Due to its high importance, it remains a great interest of scientist to develop automated methods for identifying nuclear structures [16] from histological images. A main method developed is [13]:

1. Initial Segmentation based on the Laplacian of Gaussians (LoG): Here entire image is processed through a multiscale LoG filter based approaches.
2. Local segmentation: In contrast to global segmentation, here only a portion of the image is processed at a time to identify specific structures. This improves initial segmentation resulting from the distance-constrained LoG.

Figure 9 illustrates an example of Nuclear Segmentation operation on digital WSI.

2.2.3 Feature extraction

This third stage entails the extraction of object level and topological features from the nuclear-segmented image. Object level features correspond to physical appearance of cell nuclei while topological features are related to inter cell structure being formed by the

arrangement of multiple cells in a particular region [17]. Object level features can be separated in to categories such as shape, size, radiometric & densitometric, texture, and chromatin-specific [13]. Here size and shape are real object level features while others are considered to be low level features. The example of topological features includes graph based properties such as minimal spanning tree, connected components, k-NN [18, 19] graph etc. Topological features are used to formulate tissue states and also to compare different tissues by formulating matrices from this graphs and classifying values. In addition to object and topological features various statistic features such as mean, median, minimum, maximum, standard deviation, skewness, and kurtosis can also be used for classification purpose. Normally, for binary image number of features are in order of 100 but for RGB image these features are extracted for each R, G & B channel separately, hence the number of features can easily exceed 1000 [13]. In classical approach, feature extraction process is typically followed by final classification stage where classification models such as Support Vector Machine (SVM) and Random Forest (RF) are developed to classify these features in to two or more categories based on the nature of the problem under consideration [20, 21].

2.3 Deep Learning

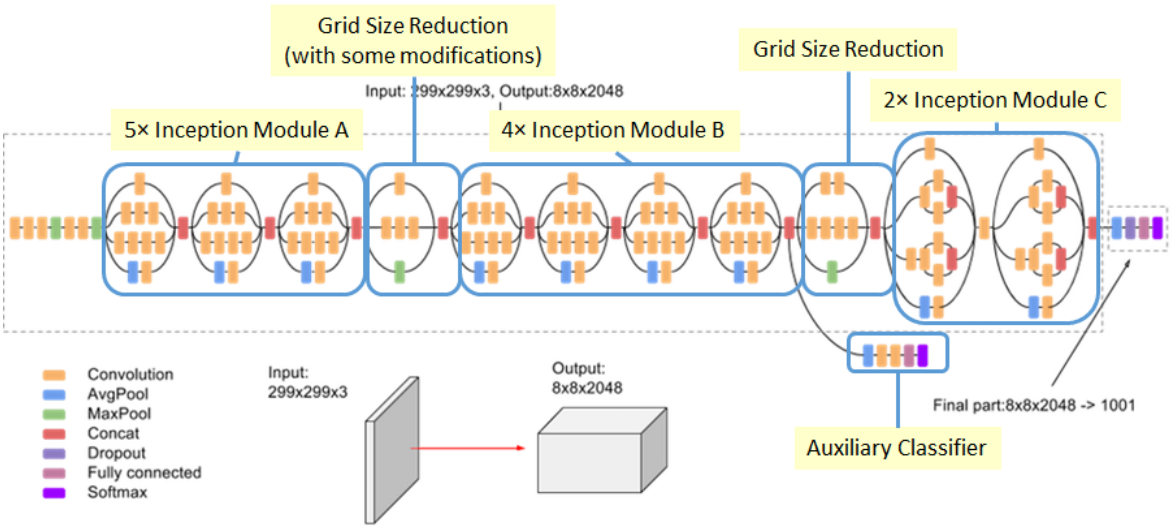

Figure 10: Inception-v3 Architecture with Batch Norm and ReLU used after Conv [25] (from Sik-Ho et al.)

In recent years, deep learning using CNNs, have been extensively explored in image analysis. CNNs can learn high dimensional useful features from image patches by leveraging loss function in the optimization process. These deep learning methods have achieved significant performance improvement in image analysis, especially on histological image analysis. For instance, a CNN framework, that takes full advantage of recent Inception architecture [22] *Figure 10*, was proposed for detecting breast cancer metastasis in lymph nodes on gigapixel pathology images [23].

The deep network takes a gigapixel image as input, and then classifies and localizes tumors for a pathologist's review. The method shows competitively performant results by correctly detecting 92.4% of the tumors in the images.

A CNN based novel architecture was also proposed, named BiCNN, for classifying breast cancer on histological images. The BiCNN showed high accuracy (up to 97%) in cancer

classification by including an advance data augmentation method through transfer learning [24].

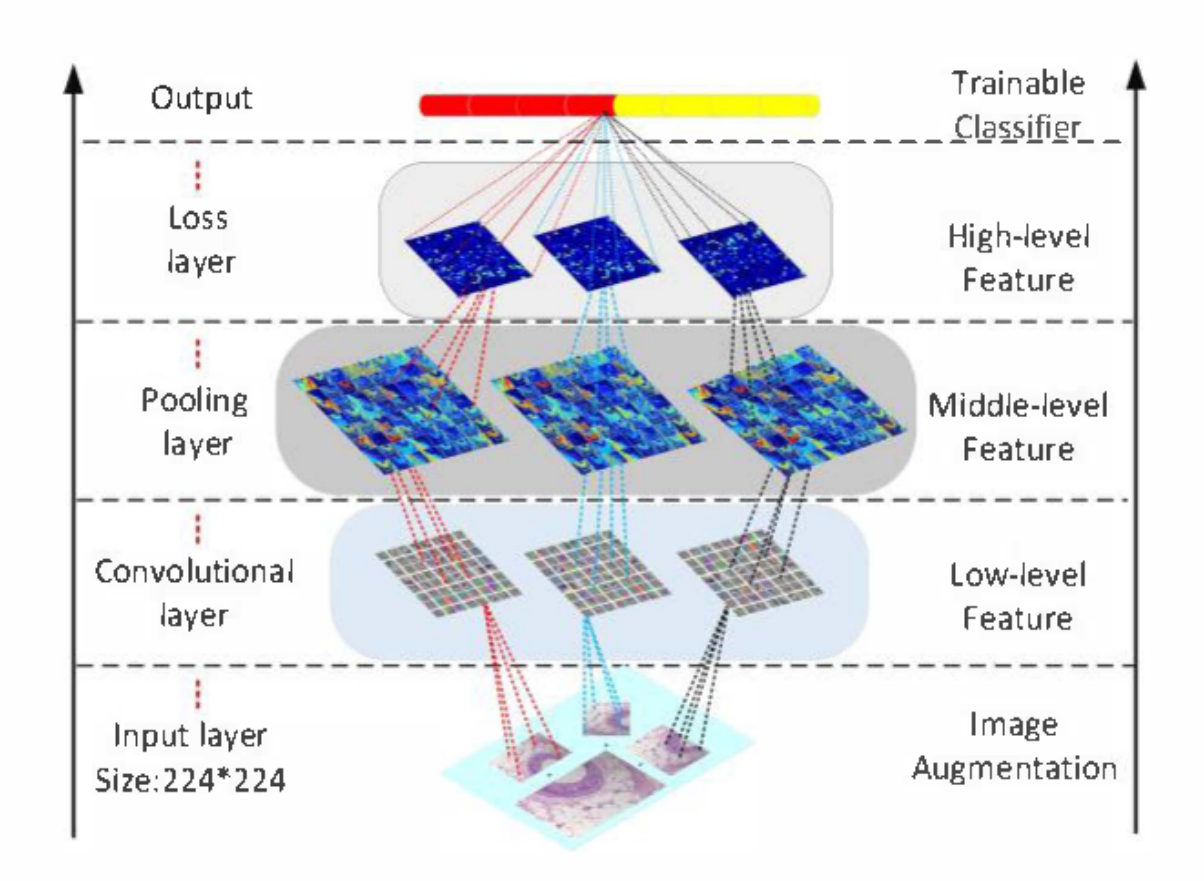

Figure 11: The BiCNN with end-to-end feature learning of lower-to-higher level layers [24] (from Wei Benzheng et al.)

A Multiple Instance Learning based CNN model was also proposed and applied on multi-gigapixel whole slide images (WSIs) to classify glioma subtype [25]. The model is trained by iteratively identifying discriminative patches in the WSIs. Additionally, the model robustly analyzes the discriminative patches through Gaussian smoothing.

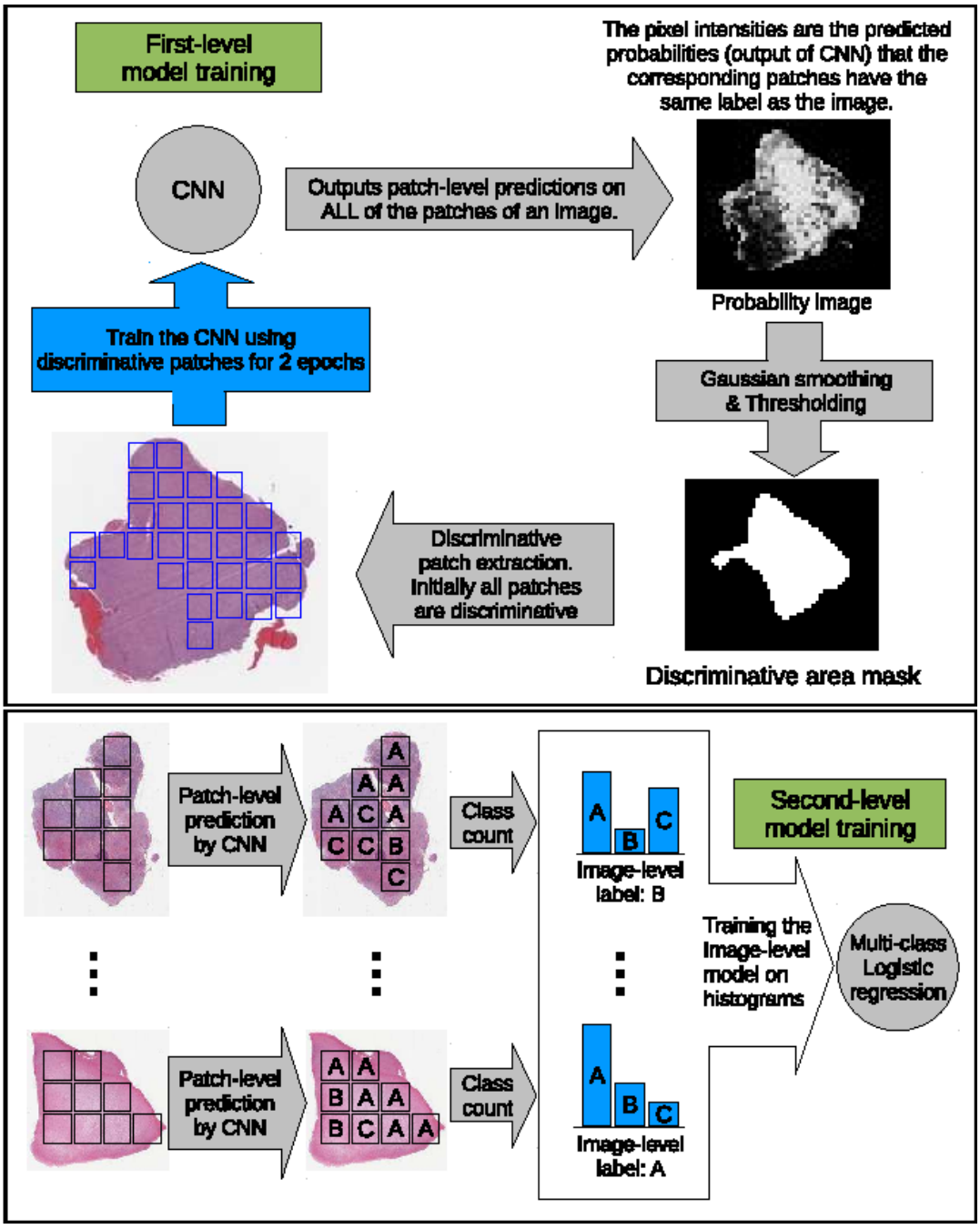

Figure 12: An overview of the BiCNN workflow [25] (From Hou L et al.)

All these works ultimately solve the task they are meant for, have a number of common flaws faced by Deep Neural Networks: the curse of dimensionally, the necessity for huge computational resources, data labeling, and the problem of overfitting as the model goes deeper.

CHAPTER 3: PROPOSED METHOD

3.1 Whole Slide Image (WSI) classification pipeline

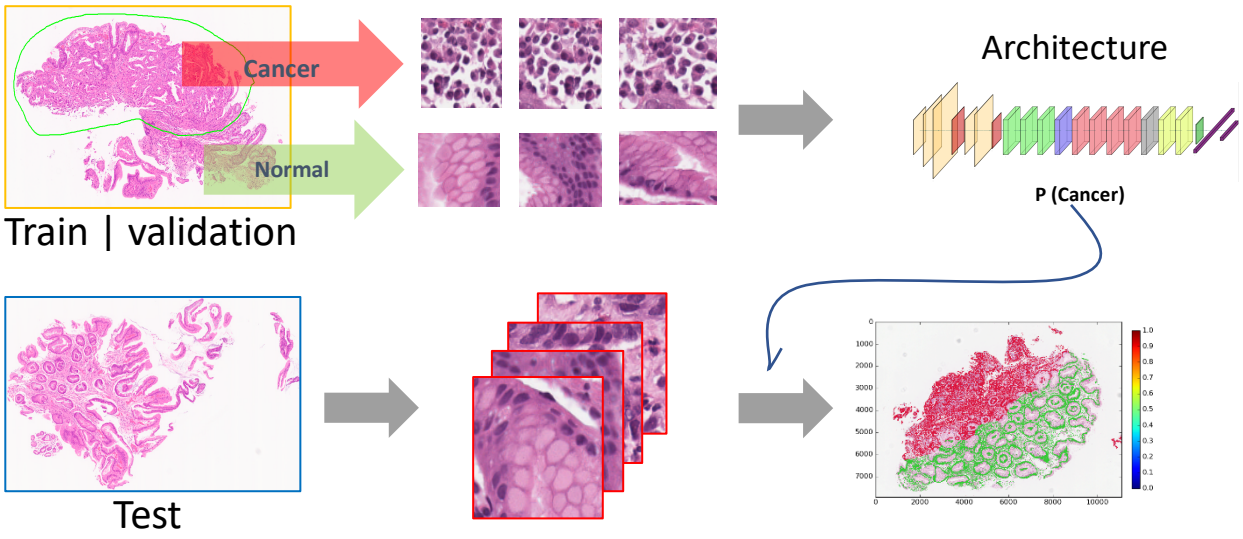

Figure 13: Cancer Texture (CAT-Net) Framework

In this report, we attempt to overcome the challenges faced by classical methods with the development of a Deep Learning based classification pipeline for identifying carcinoma cancer from digital WSI. Our classification pipeline consists of four stages:

1. Image preprocessing for Region of Interest (ROI) detection
2. Training the Deep CAT-Net model for tile-based classification
3. Building tumor probability heat-maps using trained model
4. Post-processing on heat-maps for slide-based classification

Figure 13 depicts our carcinoma cancer detection framework

3.2 Image preprocessing for Region of Interest (ROI) detection

The goal of WSI preprocessing is to localize tissues within the WSI and exclude back ground. A primary motivation for this is the reduced computational time and avoiding outliers, while focusing on slide regions most likely to contain carcinoma. The first stage in our pipeline is to identify the regions of interest annotated by digital pathologists into two main class: Regions with high potential of containing cancer and regions with very low potential of containing cancer. Then we identify tissue region (foreground) from respective regions of the whole slide image by excluding background white space. As described before, WSIs are very large GigaPixel (~10^6 x ~10^6 pixels) images thus processing even a single image takes a significant amount of time [26]. Finding ROI is an essential step as it helps to reduce computation time to a great extent by allowing to process only the region where probability of having tumor is more likely [3]. Similar to [3], we were able to remove approximately 85% of background region per WSI. Python open-CV APIs are used to perform various operations involved in finding ROIs. Preprocessing includes five steps:

1. Cancer/Normal region segmentation: This is the first stage in our preprocessing. It consists of grouping the WSI into two regions, following its corresponding XML annotation file. The first region is where the tumor is most probable to occur, and the second region contains normal cells with very low tumor probability. This first hand analysis by pathologist, enables us to know where to extract right ground truth for classification.

2. **RGB to HSV conversion**: This step entails converting the original image from RGB color space to HSV (hue, saturation and value) color space. In HSV color space, analyzing color values is more convenient as values are more intuitive and easy to represent.

3. **Binary mask generation**: Next step is to build a binary mask by filtering H, S & V component values in a set range. Specifically, we filtered pixels having values in the range 40 to 205 of H, S & V components. In industry, threshold based technique provided by Otsu's technique provided by Open CV is quite popular for generating binary masks but we have developed our own method based on filtering pixel values, given that it produces better results compared to Otsu. The binary mask contains white pixels in areas where pixel values falls within the filtered range and black pixels everywhere else.

4. **Finding contours**: The last operation is to find contours from the binary mask obtained. This operation derives the boundaries of white areas in the binary mask. After finding contours we draw them onto the original RGB image in order to highlight ROIs.

The complete process of ROI detection and final results, are visualized in *Figure 14*:

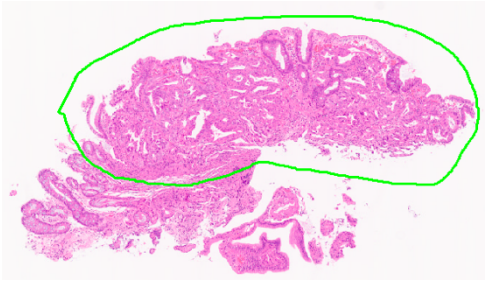

A: Annotated input data

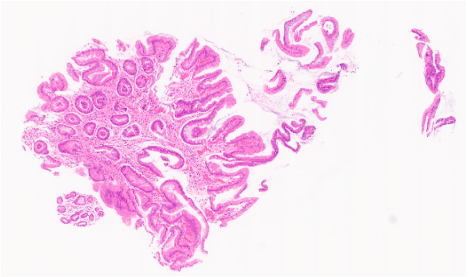

B: Extracted region from input annotations

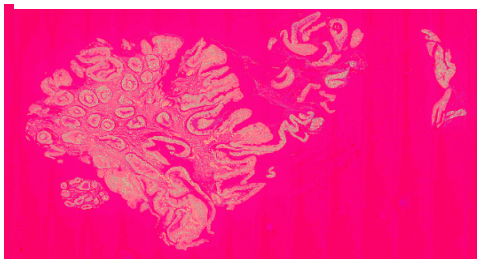

C: HSV conversion to enhance filtering

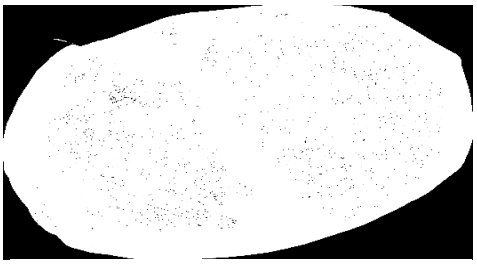

D: Generated mask to exclude noise and background

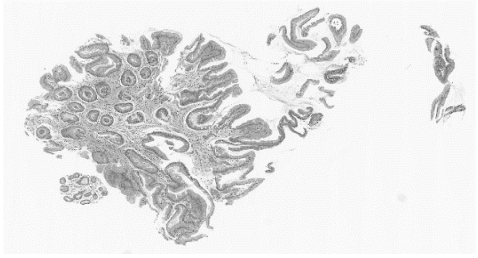

E: Resulting ROI for tiling window based on Mask

Figure 14: ROI Detection Process: Original image (A) ➔ region segmentation (B) ➔ HSV (C) ➔ filtered mask (D) ➔ output (E)

3.3 Training data construction: Tiling ROI

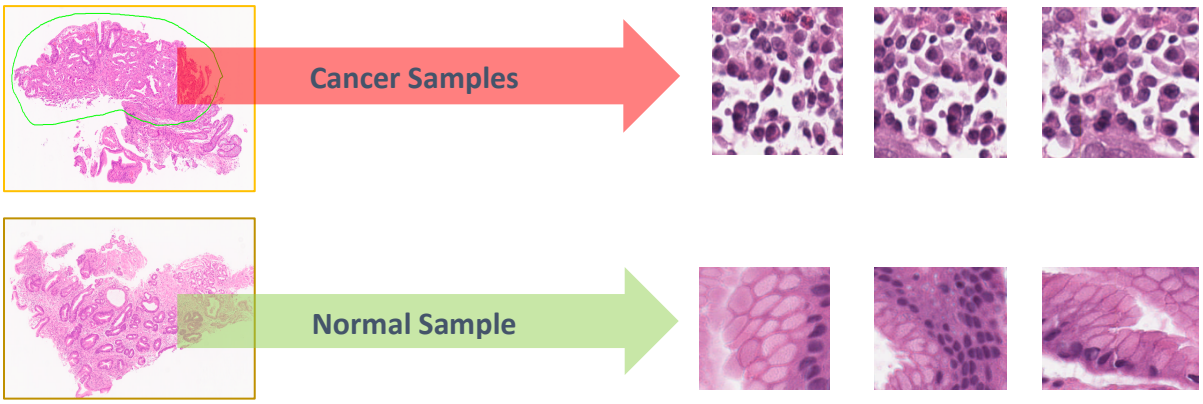

Figure 15: Patch extraction from WSI. Tumor regions are highlighted within the green annotations, while the remain regions contain normal tissues

This section explains the details about construction of training set, to be used for training Deep model. For the Deep learning setting, the dataset is repartitioned into training, validation and testing in the ration 2: 1: 1 respectively. WSIs are very large GigaPixel images, with resolution of ~10^6 x ~10^6 pixels and raw size of more than 50GB. Because of large size, it is impossible to load a full image into a computer memory, which makes it infeasible to analyze an entire whole image at once. Due to this limitation, we decided to perform patch based analysis. We randomly extracted thousands of 256 x 256 size patches from ROIs of each WSI image [27], ~3k tumor & ~1k normal patches from each Tumor slides and ~4k normal patches from each Normal slides. In total we extracted (~249k)*2 patches, (~162k)*2 normal patches and (~87k)*2 tumor patches. We multiply each amount by two because for every one WSI of Hematoxylin and Eosin (HE) stain, there is a corresponding duplicate stained with Cytokeratin (CK). *Figure 15* demonstrates the process of extracting patches in detail. Data augmentation techniques is applied to train the model with increasing variety of data and to avoid overfitting of training data. We randomly crop a 224 x 224 sub-region from original patches or flip patches horizontally as shown in *Figure 16*.

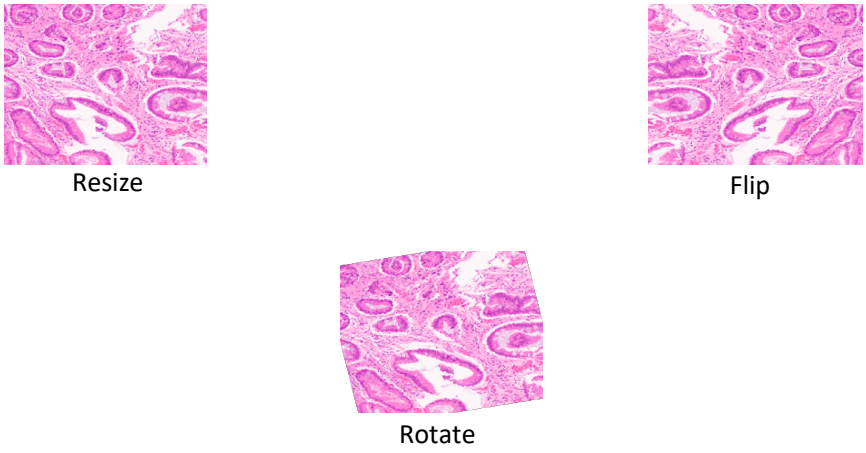

Figure 16: Data Augmentation

3.4 Cancer Texture Network (Cat-Net) Model for tile-based classification

Convolutional neural networks are powerful deep learning based approaches for visual recognition tasks. Starting 2012, major image classification challenges such as ImageNet has been consistently won by deep learning based approaches every year. Recently, deep learning based approaches have also shown state-of-the-art results in medical science challenges such as MICCAI 2013, 2018, BIBM 2018 and even the Data Science Bowl Kaggle Competition, which shows the potential of applying deep learning to solve real life health care related problems in clinical practices [28]. Classical machine learning based approaches require lots of manual steps for object detection, object segmentation and feature extraction, while deep learning based approach automatically learns high-dimensional complex features just with the use of training data and its labels (e.g. 0 and 1) [3]. In cancer pathology, mitosis detection is a very important process as mitosis count is a key indicator of presence and severity of cancer disease.

Traditionally, mitosis count has been performed by pathologist but it is a very time consuming process because pathologist has to scan millions of tissues manually. Automating this process has high value in clinical practices because it would be faster, cheaper, more accurate, and more reliable. Classical computing methods developed for mitosis counting are based mainly on pixel classifiers and detecting particular objects from the images. Mitosis detection is quite a challenging process as it is very hard to distinguish between mitotic and non-mitotic nuclei [28]. Thus scientists start developing Convolutional

Network based approach for mitotic detection to lever the process of mitosis detection with less effort. As stated by [3], Convolutional Networks yield robust hierarchies of features unlike computer vision approaches that rely on hand crafted features from images and videos. However, tasks like tumor segmentation in computer aided diagnosis must be practically accurate to each pixel and hence raises the need for robust and highly accurate methods.

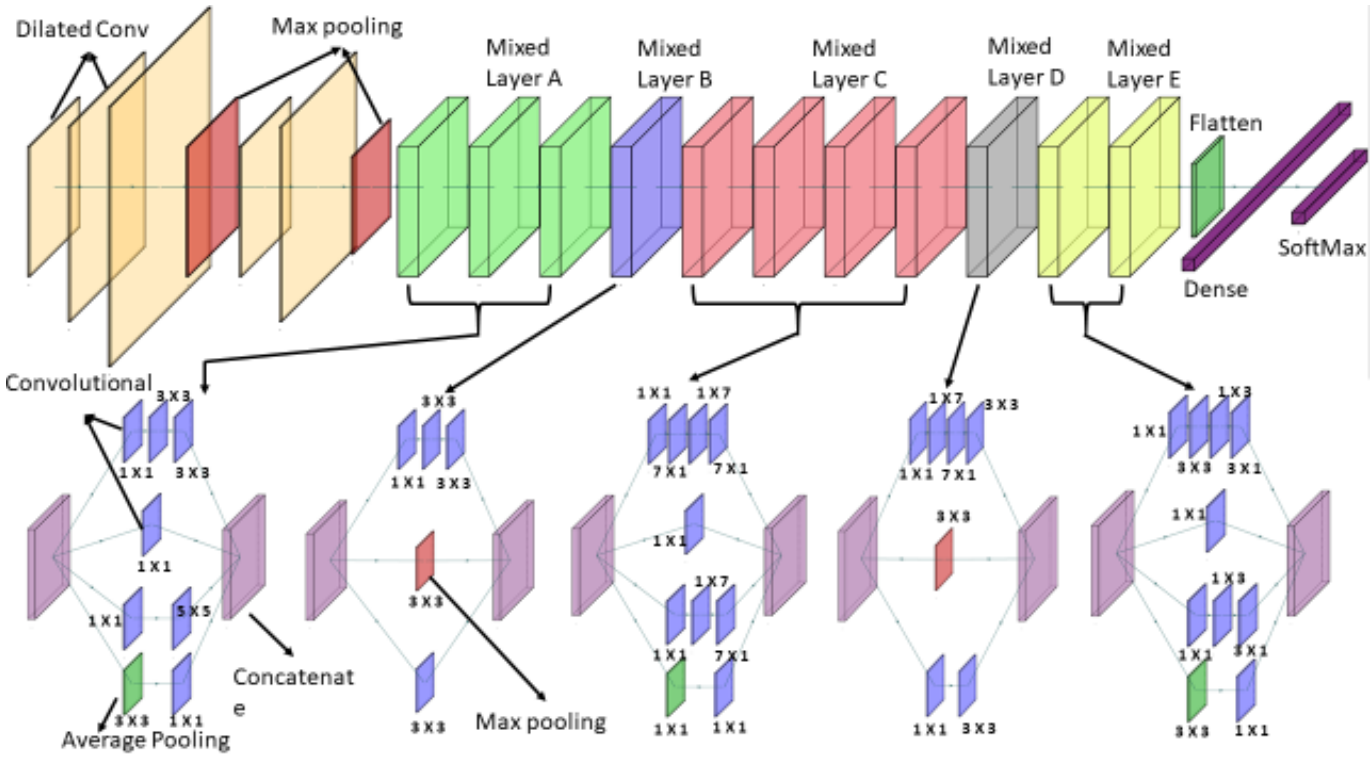

Figure 17: CAT-Net Architecture

This section explains the use of a Deep Convolutional Networks - Cancer Texture Network (CAT-Net) for patch based classification. We trained the Deep classification model from scratch to distinguish between positive carcinoma cancer and Negative patches. Table 2 displays the detailed information about training CAT-Net. During training, our model uses as input 256 x 256 size patches extracted from positive and negative regions of WSIs as explained in section 3.3. We apply the "no free lunch (NFL) theorem" and evaluate the performance of many well-known deep learning network architectures for this classification task, then adopt CAT-Net (inspired by Google's Inception-V3 deep learning model due to its fastness and stability compared to other networks) as our deep network structure. CAT-Net structure consists of 27 layers in total and more than 6 million parameters [29]. Table 2 lists detailed information about CAT-Net including types of layers, patch size, stride and input size of each layer. *Figure 17* depicts layer by layer architecture of CAT-Net. For training, we used mini-batch Stochastic Gradient Descent (SGD) as optimizer with a momentum of 0.9, Softmax cross entropy as the loss function, and cyclic learning mechanism for managing the learning rate through the learning rate scheduler. We set initial learning rate to 0.002 and decreased the value by the factor of 7 after every 7 iterations, in order to reduce oscillation and avoid divergence during model training. We also use batch-normalization [30] to achieve faster training and drop-out [31] to avoid overfitting of training data. Using this setup, we train deep CAT-Net model with 4 GPUs and a batch size of 10 until it converges. ***Figure 18*** illustrates the training loss progress while training Deep CAT-Net.

Table 1: Details of CAT-Net Architecture

Layer (Number)	Filter Size	Stride	Output (W×H×N)	
Dilated Conv (1)	3×3	2	256 × 256 × 3	
Dilated Conv (2)	3×3	1	149 × 149 × 32	
Dilated Conv (3)	3×3	1	147 × 147 × 32	
Max Pooling (4)	3×3	2	147 × 147 × 64	
Dilated Conv (5)	1×1	1	73 × 73 × 64	
Dilated Conv (6)	3×3	1	73 × 73 × 80	
Max Pooling (7)	3×3	2	71 × 71 × 192	
MixedA (8)	(1×1) (3×3) (5×5)	1	35 × 35 × 192	
Mixed layer A (9)	(1×1) (3×3) (5×5)	1	35 × 35 × 256	
Mixed layer A (10)	(1×1) (3×3) (5×5)	1	35 × 35 × 288	
Mixed layer B (11)	(1×1) (3×3)	2	35 × 35 × 288	
Mixed layer C (12, 13, 14, 15)	(1×1) (1×7)*2 (7×1)*2	1	17 × 17 × 768	
Mixed layer D (16)	(1×1) (1×7) (7×1) (3×3)		17 × 17 × 768	
Mixed layer E (17)	(1×1) (1×3) (3×1) (3×3)		8 × 8 × 1280	
Mixed layer E (18)	(1×1) (1×3) (3×1) (3×3)	1	8 × 8 × 2048	
Average Pooling (19)	(1×1)		8 × 8 × 2048	

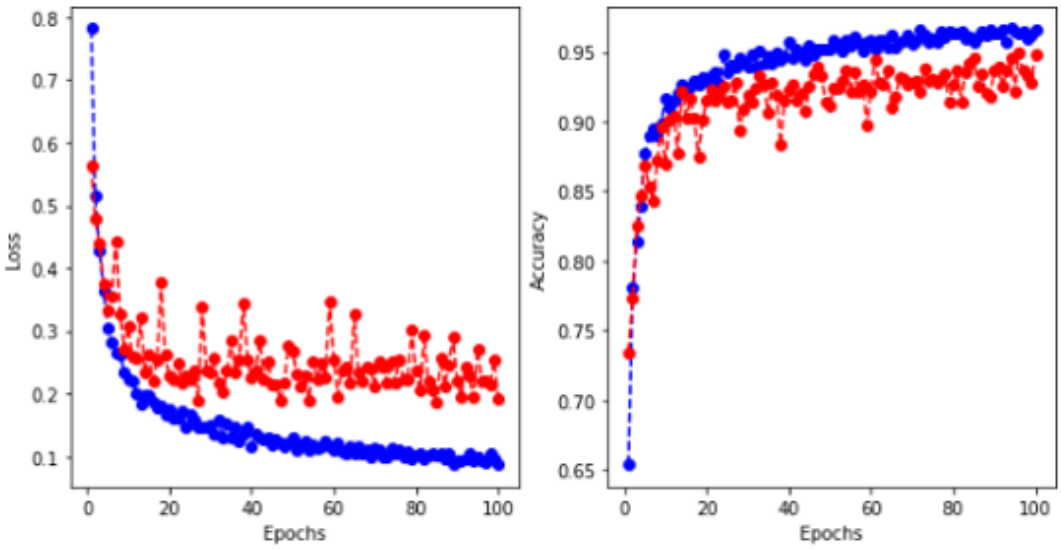

Figure 18: Training loss and accuracy in blue against validation loss and accuracy in red

Environment used for training includes:

1. CPU: 2.3GHz Intel Xeon (R)
2. GPUs: NVIDIA-SMI (410.48) Driver Version: 410.48
3. RAM：225GB
4. HDD: 10 TB

Software Requirements:

1. OS: Ubuntu 18.04

2. Programming Languages: Python 3.6

3. Deep Learning libraries: Pytorch (versioin), Skorch (Version)

4. Support libraries: OpenSlide, SciKit, NumPy, torchvision, Opencv

CHAPTER 4

EXPERIMENTAL RESULTS

4.1 Experimental Dataset

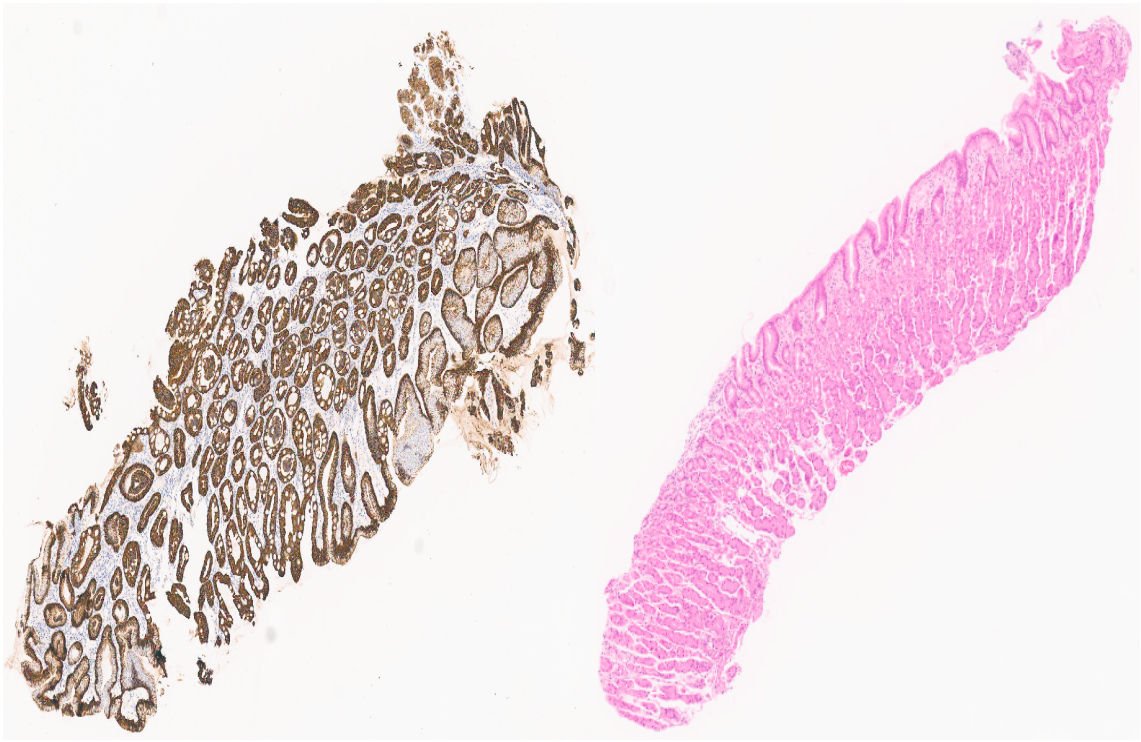

Figure 19: SWI made of Cytokeratin (CK) stains on the left and WSI made of H&E stains on the right

We obtained gastroscopic biopsy specimen of 94 cases at the Gyeongsang National University Changwon Hospital (Changwon, Korea) between February 2016 and July 2017, and the tissue specimens were stained with hematoxylin and eosin (H&E) using standard protocols in routine clinical care. This study included 188 whole slide images (WSIs) with 26, 22, 40, 40 and 60 WSIs for well, moderately differentiated adenocarcinoma, poorly differentiated adenocarcinoma, poorly cohesive carcinoma including signet-ring cell

features, and normal gastric mucosa, respectively. The histologic type and differentiation grade of the carcinoma was determined according to the classification system of the World Health Organization, fourth edition. This study was approved by the Institutional Review Board of Gyeongsang National University Hospital with a waiver for informed consent (2018-08-005-001). Out of the 188 WSIs, half (144 slides) are made of H&E stains, and the other half consist of identical slides, but made of CK stains as shown in ***Figure 19*** obtained with Aperio image scope visualizer. For H&E slides, ~249k patches are extracted, with ~162k normal patches and ~87k tumor patches as explained in section 3.3. To promote a fair environment between both classes, we select all the ~87k tumor patches, and perform a random selection without replacement of ~87k out of ~162k equivalent normal patches. We split the resulting data into a train, validation and test ratio of 2:1:1 as mentioned in 3.3.

4.2 Experimental setup

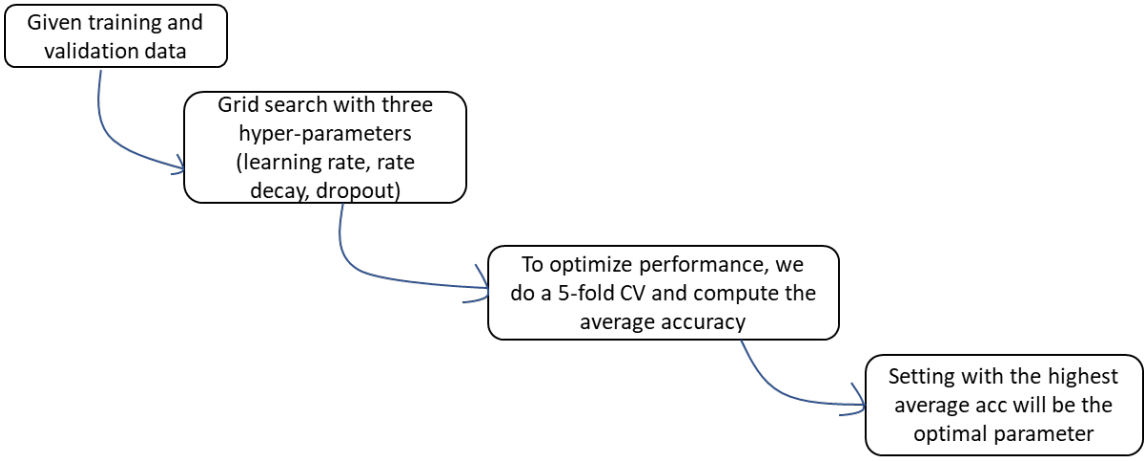

Figure 20: Experimental flow for hyper parameter search

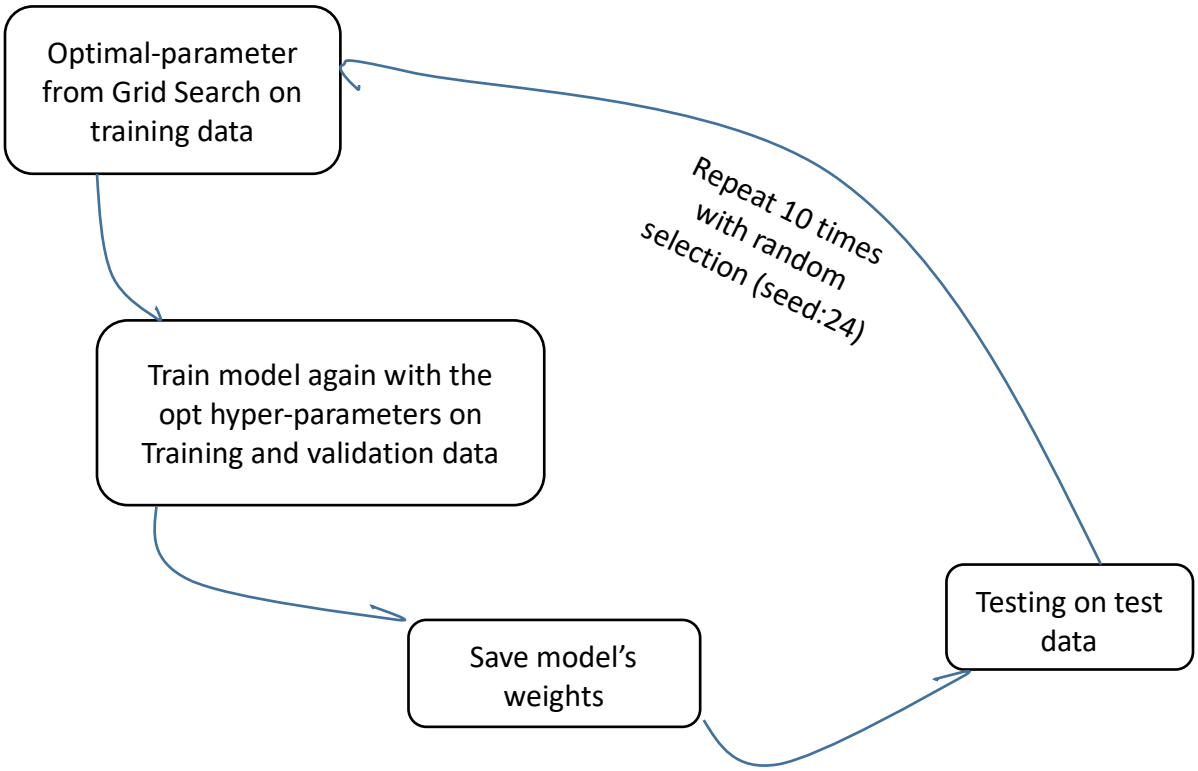

Figure 21: Experimental flow for model optimization and testing

Figure 20 and *Figure 21* demonstrates the experimental flow diagram:

To successfully perform experiments on proposed system following requirements are setup at Data X Lab. The hardware configurations of the system are:

1. CPU:3.4GHz Intel Xeon (R)
2. RAM: 12GB DDR4
3. NVIDIA (410.48) Driver Version: 410.48 GPU
4. NVIDIA (410.48) Driver Version: 410.48 GPU

The software requirements are:

1. OS: Ubuntu 18.04
2. Programming Languages: Python 3.6
3. Deep Learning libraries : Pytorch, Skorch
4. Support libraries: OpenSlide, Sklearn, NumPy, Pandas

Approximate finish time: ~ (180+90)*10 minutes = ~45hrs

4.3 Evaluation metrics

We elaborate a classification report using AUC, Precision, Recall and F1 score. AUC is the area covered by the ROC curve. The precision is number of true positive predictions, over the total positive and negative predictions in the samples space. Recall on is calculated as a ratio of true positive patches, over both the true positive and false positive patches. The F1 score is a division of two times the sum of the precision and recall over the product of the precision and recall:

$$Precision = True\ positive\ /(True\ positive + false\ positive)$$

$$\text{Recall} = True\ positive\ /(True\ positive + false\ negative)$$

$$F1_{score} = 2 * (precision * recall)/(precision + recall)$$

We focus on Recall to closely monitor the worst case scenario, which entails false negative predictions (i.e. predicting that a patient does not have cancer whereas he/she does).

4.4 Model D-1 results

4.4.1 Training

As explained in section 3.1.3, we trained Deep CAT-Net model to distinguish between tumor and normal patches. We used mini-batch Stochastic Gradient Descent (SGD) as the optimizer, Softmax cross entropy as the loss function and cyclic learning rate scheduler for learning rate. We set the initial learning rate to 0.002 and decreased the value by the factor of 7 after each X iterations, in order to reduce oscillation and avoid divergence. In order to eliminate variability in pixel intensity, we adopted standard data normalization techniques directly after the preprocessing stage in our ETL Pipeline. For each training patch, we bring the pixel intensity values to a mean of [mean] and standard deviation of [std]. These values are obtained by computing the mean and standard deviation of our training data. The values are therefore saved in the pipeline and later on applied to the validation and test data. The model is trained continually using 4 GPUs with batch size 32 until convergence is achieved. After 40 iteration, CAT-Net obtained a patch based classification accuracy of 97.8%.

4.4.2 Metric performance

We compare our results with 3 main state-of-the-art models: GB INCV3 (Google Brain Inception V3 [23]), N-Net50 [32], N-Net256 [32], VGG16 [3] and report a higher performance from CAT-Net model, upon comparing each model in the same experimental setup, based on our defined performance metrics.

1. GB INCV3: The kernel window of 299 by 299 pixels with stride of 128 pixels was slid on the WSIs to generate patches, as proposed. GB INCV3 was implemented by its open source in Tensorflow provided by the authors, where Adaptive Moment Estimation (Adam) optimizer was used. The optimal hyper-parameters of learning rate, dropout, and weight decay were obtained by grid search with training and validation data on each experiment.

2. N-Net50: To directly compare the performance, the non-overlapping window of 50 by 50 pixels was used to generate patches without nuclei segmentation. We implemented N-Net using Keras in Python, where Stochastic Gradient Descent (SGD) optimizer was used. The optimal hyper-parameters were obtained in the same manner as in GB INCV3.

3. N-Net256: N-Net was also trained with the same size's patches (256 by 256 pixel) inputs with CAT-Net.

4. VGG16: We trained a WSI patches with 256 x 256 with VGG16 architecture as proposed in [3]. We implemented VGG16 using Keras in Python, where SGD optimizer was used. The optimal parameters were obtained with same manner as GB INCV3. The optimal hyper-parameters were obtained with the same manner with GB INCV3.

The table below provides the experimental results of CAT-Net against the stated deep learning approaches all performed in the same experimental setting on the same data.

Table 2: Experimental Results

Method	Accuracy*	Precision	Recall	F1 score
GB INCV3	0.937 (0.0042)	0.938 (0.0042)	0.936 (0.0033)	0.937 (0.0046)
N-Net50	0.603 (0.0080)	0.696 (0.0042)	0.692 (0.0080)	0.693 (0.0090)
N-Net256	0.662 (0.0034)	0.664 (0.0054)	0.663 (0.0052)	0.663 (0.0045)
VGG16	0.682 (0.0120)	0.674 (0.0091)	0.689 (0.0130)	0.681 (0.0110)
CAT-Net	**0.961 (0.0029)**	**0.965 (0.0052)**	**0.961 (0.0031)**	**0.962 (0.0055)**

**All numbers in the table are shown as average (standard deviation) of ten experiments*

4.5 Building Tumor probability heat-map

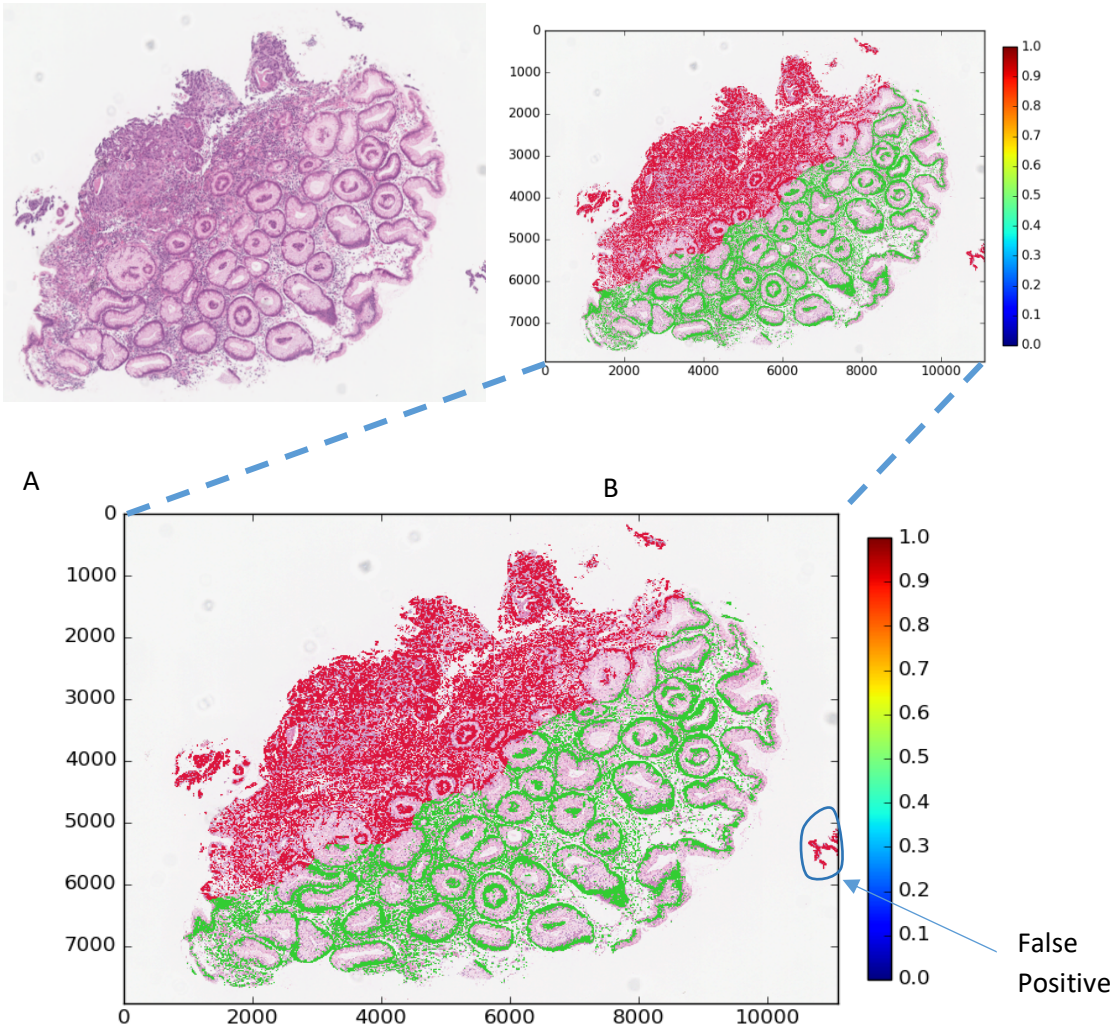

Figure 22: A is the original input image and B is the output tumor probability heat map. C is a zoomed version of B.

A heat map is a representation of data in the form of a map, in which the data values are represented in colors. During testing, the sample WSI is ingesting into the same ETL pipeline built for the training data, consisting of data preprocessing, tiling and batch normalization. A sample test slide contains an average of 1888 tile images of size 256*256 extracted at 40x magnification level. Upon inference, these tile images are assigned a probability score between 0 and 1 depending on how like it is tumor or not as shown in ***Figure 22***. These probability scores are saved and then visualized as a heat map, with each tile having a color representative of its score. An inconvenience with our model was the fact that it produced much false positive, making it sometimes difficult to distinguish Normal WSI heat-maps from Tumor WSI heat-maps. These false positives are due incomprehensive training data as we randomly extracted normal training patches to reduce the number of normal training samples. Due to this randomness, some negative (normal) patches whose texture could not be accurately captured happened to mimic positive (Tumor) patches. ***Figure 22*** shows an example of false positive in CAT-Net's heat-map when zoomed in. To remove false positives, we adopted a stratified K-fold cross validation, during which equal number of classes could be selected throughout the negative and positive tiles without replacement. This enabled a better capture of the texture for negative tiles, hence an improved performance.

4.6 Post-processing on heat-maps for slide-based classification

After assigning a tumor probability score to each tile in a slide visualized on a heat map, another challenging task is to assign a fixed probability score to the complete WSI. This process entails completing the classification pipeline, with a unique score assigned to a WSI containing ~10^6 * ~10^6 features.

With approximate 1888 probability scores between 0 and 1 produced by a SWI, we adopt K-mean clustering on all the 1888 new features on each slide, to assign a single score. The number of K clusters is determined using the Elbow method. The Elbow method consist of fitting our new features (scores) in a considerable range of clusters values (1 to 10 in our case), then plotting the score provided by each cluster based on the resulting inter- and intra- cluster distance. The resulting curve is known as the Elbow curve. The cluster producing the largest intra- cluster distance and smallest inter- cluster distance is chosen as the best K for clustering. This value generally occurs at the elbow region of the curve, hence the name “Elbow curve”. In our case, the best K is 4 clusters as shown in ***Figure 23***.

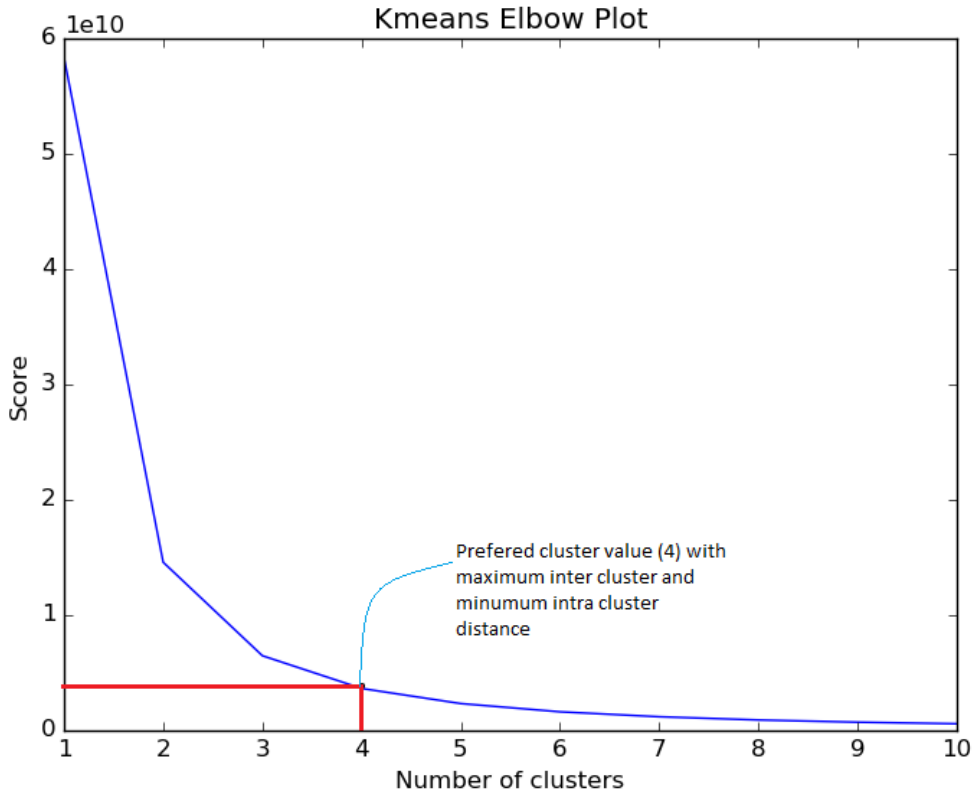

Figure 23: Choice of best K for slide classification through the elbow method on KMeans

After clustering the scores into K clusters, the cluster with the maximum amount of candidates is chosen, and the centroid of this cluster is set to be the Tumor probability of the WSI.

CHAPTER 5

IMPLEMENTATION

This project is deployed as an ETL pipeline consisting of three phases: data preprocessing phase, training phase and testing phase.

5.1 Data Preprocessing

During this phase, we identify our regions of interest (ROI) and extract the tiles from the WSI, these tile are partitioned into their respective directories, where they are later on normalized cropped, rotated and stratified. Following are the GitHub files related to preprocessing:

- load_svs.py: Parse through the XML file of the corresponding WSI and segment the ROIs for both positive and negative classes.
- load_good_svs.py: Extracts negative ROI from completely negative WSI to enable an equal distribution of both positive and negative samples over all WSIs.

  Follow the GitHub link (https://github.com/Tsakunelson/Cancer-Texture-Network/tree/master/data_preprocessing)

5.2 Training

The model architecture is created, hyper parameters choosing through grid search and then trained with input training data, and validated with validation data, following our set performance metric standards:

- load_data.py: Generates fixed size patches from the extracted ROIs, apply normalization with calculated mean and standard deviation, perform data augmentation, transform into tensors, and loads the results into the network, following a fixed batch size.
- gridSearchSkorch.py: A hyper parameters search strategy, similar to Sklearn's grid search module. The outcome here provides the optimal hyper parameters, necessary to provide the most favorable performance.
- cat_net_model.py: This is the model architecture. It takes tensors as input and release a single class score as output.
- cat_net_model_spatial_pyramid_pooling.py: This is the second version of our model architecture. Added the first model is its ability to ingest variable size of tensors as input, due to its spatial invariance nature, realized with Atrous Spatial Pyramid Pooling [33]

  Follow the GitHub link (https://github.com/Tsakunelson/Cancer-Texture-Network/tree/master/Training)

5.3 Testing

For inferencing, we pass our data through the same data preprocessing steps performed on training data, such as normalization with mean and standard deviation. We later test the data which is initially independent of training data and further provided a heat-map as explained in section 4.5.

- Predict.py: Applies the set transformations from training data to incoming data though an established Extract Transform Load Pipeline. Then makes a class prediction on the transformed data.
- Heat_map.py: A visual representation of the probability score for each patch in the WSI all brought together for a combined score of the complete WSI

  Follow the GitHub link (https://github.com/Tsakunelson/Cancer-Texture-Network/tree/master/Inferencing)

CHAPTER 6

CONCLUSION AND FUTUR WORK

The purpose of this thesis is to present a deep learning based system for automated detection and classification of carcinoma cancer from stomach epithelial cells, expressed on whole slide images. The main challenges of the system was hyper-parameter tuning of the architecture for the optimal model to overcome current state-of-the-art models. Another challenge was to enhance the training set to improve the previous systems by avoiding misclassification (false positive) of the normal lymph node regions as cancer. Other important key features of the system were to develop state-of-the art deep learning architecture to classify small patches from the large whole slide images, and use of carefully designed post-processing methods for the slide based classification. Classical methods in histopathology are mainly focused on image analysis tasks such as color normalization, nuclear segmentation, and feature extraction [3]. Usually, image analysis task alone is not sufficient for cancer classification; so in practice after image analysis, machine learning based classification models such as Support Vector Machine and Random Forest are required for end-to-end feature classification task. Since many years, deep learning-based approaches have played a major role in various computer vision competitions, such as ImageNet Large Scale Visual Recognition Competition (ILSVRC). Recently Deep-learning has also emerged as a leading technology in the field of pathology and related research areas in medical science [28]. For instance in 2018, the Data Science Bowl Kaggle competition was hosted, with purpose to created deep learning algorithms to

accurately detect and segment nuclei cells, which would create great advancements in medical research.

In contrast to classical machine learning based approaches, deep-learning based approach does not require manual steps for object detection, object segmentation and feature extraction as it automatically learns high-dimensional complex features, just with the use of training data and its labels (e.g. 0 and 1) [3]. The proposed method CAT-Net is inspired from GoogLe's Inception model, a 27-layer deep network architecture. CAT-Net improves the performance by capturing multi-scale cancer texture patterns from a WSI. Comparing to the Inception model, CAT-Net does not include an auxiliary classifier. CAT-Net leverages the first part of the inception module without computing an auxiliary loss, which reduce models complexity while preserving the performance. CAT-Net produced outstanding performance among the current state-of-the-art methods in cancer histopathological image classification. CAT-Net obtained near human- level classification performance on carcinoma cancer test data. As tested by [33], the errors made by deep learning based systems are not strongly correlated with the errors made by human pathologist. Thus, although the pathologist alone is currently superior to deep learning system alone, combining deep learning with the pathologist produced a major reduction in pathologist error rate, reducing it from over 3 percent to less than 1 percent. Based on our results, we can conclude that integrating deep-learning based approaches into clinical practices can bring vast improvements in speed, accuracy, reproducibility, reliability and clinical value of pathological diagnoses. ***Figure 24*** shows Feature maps which are extracted from CAT-Net illustrating the distinctive texture patterns of cancer and normal on WSIs.

A future research direction could be to train and evaluate the performance of our system on another large scale open source cancer data such as TCGAs lung cancer dataset. Another important step in future research would be to integrate staining normalization process into proposed classification pipeline. Stain normalization is a crucial part of building a generalized deep learning model for identifying carcinoma cancer in stomach regions as it eliminates the stain variability in WSIs, induced by different staining techniques. As shown by [34], stain normalization process has a great potential to significantly improve classification performance of a deep model, which indicates that with stain normalization on board, proposed system could produce even better results and could be extended to any carcinoma cancer digitized images without institutional re-calibration.

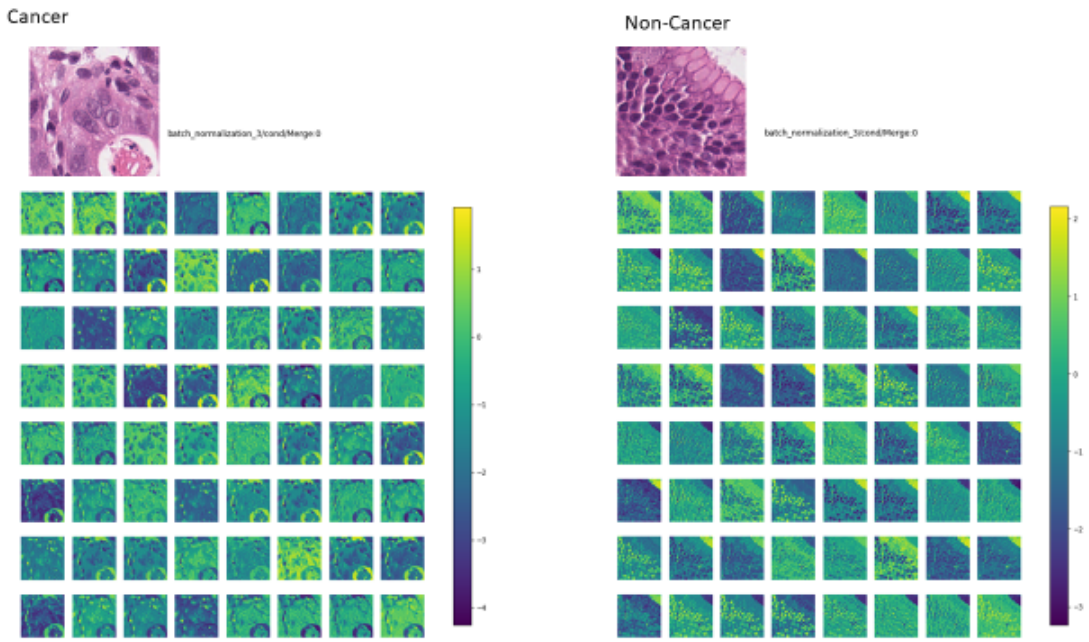

Figure 24: Feature map of a sample Cancer (left) and non-cancer (right) patch

References

[1] Y. Jiawen, W. Sheng, Z. Xinliang and H. Junzhou, "Imaging biomarker discovery for lung cancer survival prediction," in *MICCAI 2016*, Athens, Greece, 2016.

[2] Z. Xinliang, Y. Jiawen, Z. Feiyun and H. Junzhou, "Making Survival Prediction from Whole Slide Pathology Images," in *CVPR*, 2017.

[3] D. Wang, A. Khosla, R. Gargeya, H. Irshad and A. Beck, "Deep Learning for Identifying Metastatic Breast Cancer," in *arXiv:1606.05718*, 2016.

[4] C. Callau, C. Callau, M. Lejeune, A. Korzynska, M. García, G. Bueno, R. Bosch, J. Jaén, G. Orero, T. Salvadó and C. López, "Evaluation of cytokeratin-19 in breast cancer tissue samples: a comparison of automatic and manual evaluations of scanned tissue microarray cylinders," *BioMedical Engineering Online,* vol. 14, 2015.

[5] B. Czerniecki, A. Scheff, L. Callans, F. Spitz, I. Bedrosian, E. Conant, S. Orel, J. Berlin, C. Helsabeck, D. Fraker and C. Reynolds, "Immunohistochemistry with pancytokeratins improves the sensitivity of sentinel lymph node biopsy in patients with breast carcinoma," *Cancer,* vol. 85, no. 5, 1999.

[6] C. Richard, J. Yating and J. Hunter, "Identifying Metastases in Sentinel Lymph Nodes with Deep Convolutional Neural Networks," p. 5, 4 08 2016.

[7] L. Hou, D. Samaras, T. M. Kurc, Y. Gao, J. E. Davis and J. H. Saltz, "Patch-Based Convolutional Neural Network for Whole Slide Tissue Image Classification," 2016.

[8] K. Oikawa, A. Saito, T. Kiyuna, H. Graf, E. Cosatto and M. Kuroda, "Pathological diagnosis of gastric cancers with a novel computerized analysis system," *Journal of Pathology Informatics,* vol. 8, no. 5, 2017.

[9] E. Cosatto, P.-F. Laquerre, C. Malon, H.-P. Graf, A. Saito, T. Kiyuna, A. Marugame and K. Kamijo, "Automated gastric cancer diagnosis on H&E-stained sections; ltraining a classifier on a large scale with multiple instance machine learning," 2013.

[10] H. Sharma, N. Zerbe, D. Heim, S. Wienert, S. Lohmann, O. Hellwich and P. Hufnagl, "Cell nuclei attributed relational graphs for efficient representation and classification of gastric cancer in digital histopathology," 2016.

[11] R. C. Gonzalez and R. E. Woods, Digital Image Processing 3ed, 2013.

[12] M. N. Gurcan, L. E. Boucheron, A. Can, A. Madabhushi, N. M. Rajpoot and B. Yener, "Histopathological Image Analysis: A Review," *IEEE Reviews in Biomedical Engineering,* 2009.

[13] H. Irshad, A. Veillard, L. Roux and D. Racoceanu, "Methods for nuclei detection, segmentation, and classification in digital histopathology: a review-current status and future potential," in *IEEE Review Biomedical Enfineering*, 2014.

[14] J. Vicory, H. D. Couture, N. E. Thomas, D. Borland, J. S. Marron, J. Woosley and M. Niethammer, "Appearance normalization of histology slides," *Computerized Medical Imaging and Graphics,* 2015.

[15] Z. Xu and J. Huang, "Detecting 10,000 cells in one second," 2016.

[16] Z. Xu and J. Huang, "Efficient lung cancer cell detection with deep convolution neural network," 2015.

[17] J. Yao, D. Ganti, X. Luo, G. Xiao, Y. Xie, S. Yan and J. Huang, "Computer-assisted diagnosis of lung cancer using quantitative topology features," 2015.

[18] F. Zhu, Y. Wang, S. Xiang, B. Fan and C. Pan, "Structured Sparse Method for Hyperspectral Unmixing," *ISPRS Journal of Photogrammetry and Remote Sensing,* 2014.

[19] G. Cheng, Y. Wang, F. Zhu and C. Pan, "Road extraction via adaptive graph cuts with multiple features," 2015.

[20] G. Cheng, F. Zhu, S. Xiang and C. Pan, "Road Centerline Extraction via Semisupervised Segmentation and Multidirection Nonmaximum Suppression," *EEE Geoscience and Remote Sensing Letters,* 2016.

[21] G. Cheng, Y. Wang, Y. Gong, F. Zhu and C. Pan, "Urban road extraction via graph cuts based probability propagation," 2014.

[22] C. Szegedy, V. Vanhoucke, S. Ioffe, J. Shlens and Z. Wojna, "Rethinking the Inception Architecture for Computer Vision," 2016.

[23] L. Yun, G. Krishna, N. Mohammad, E. D. George, K. Timo, B. Aleksey, V. Subhashini, T. Aleksei, Q. N. Philip, S. C. Greg, D. H. Jason, P. Lily and C. S. Martin, "Detecting Cancer Metastases on Gigapixel Pathology Images," 08 March 2017.

[24] B. Wei, Z. Han, X. He and Y. Yin, "Deep learning model based breast cancer histopathological image classification," 2017.

[25] L. Hou, D. Samaras, T. Kurc and Y. Gao, " Efficient Multiple Instance Convolutional Neural Networks for Gigapixel Resolution Image Classification," *arXiv preprint arXiv: ...,* 2015.

[26] R. Li and J. Huang, "Fast regions-of-interest detection in whole slide histopathology images," 2015.

[27] F. Zhu and B. Fan, "10,000+ Times Accelerated Robust Subset Selection (ARSS)," *arXiv,* 2014.

[28] D. C. Cireşan, A. Giusti, L. M. Gambardella and J. Schmidhuber, "Mitosis Detection in Breast Cancer Histology Images with Deep Neural Networks BT - Medical Image Computing and Computer-Assisted Intervention – MICCAI 2013," 2013.

[29] Camelyon 2016 grand challenge, "Camelyon 2016 grand challenge Data," IEEE International Symposium on Biomedical Imaging, 11 2016. [Online]. Available: https://camelyon16.grand-challenge.org/Data/. [Accessed 05 07 2019].

[30] I. Sergey and S. Christian, "Batch Normalization: Accelerating Deep Network Training by Reducing Internal Covariate Shift," *arXiv,* 2015.

[31] N. Srivastava, G. Hinton, A. Krizhevsky, I. Sutskever and R. Salakhutdinov, "Dropout: A Simpfile:///Users/pinkyhsu/Desktop/Dropout A Simple Way to Prevent Neural Networks from Overfitting.pdfle Way to Prevent Neural Networks from Overfitting," *Dropout: A Simple Way to Prevent Neural Networks from Overfitting,* 2014.

[32] F. Sheikhzadeh, R. K. Ward, D. Van Niekerk and M. Guillaud, "Automatic labeling of molecular biomarkers of immunohistochemistry images using fully convolutional networks," *PLoS ONE,* 2018.

[33] D. L. Weaver, D. N. Krag, E. A. Manna, T. Ashikaga, S. P. Harlow and K. D. Bauer, "Detected and Automated Computer-Assisted Image Analysis Detected Sentinel Lymph Node Micrometastases in Breast Cancer," *Modern Pathology,* 2003.

[34] C. Richard, J. Yating and J. Hunter, "Identifying Metastases in Sentinel Lymph Nodes with Deep Convolutional Neural Networks," *arXiv,* 2016.

[35] T. Sik-Ho, "Inception-v3 — 1st Runner Up (Image Classification) in ILSVRC 2015," Medium, 10 September 2018. [Online]. Available: https://medium.com/@sh.tsang/review-inception-v3-1st-runner-up-image-classification-in-ilsvrc-2015-17915421f77c. [Accessed 05 07 2019].

Biographical Statement

Nelson Zange TSAKU received his Bachelor of Science in computer Science in 2017 from Kennesaw State University, Georgia, USA. After his bachelors, he started his Masters in Computer Science at Kennesaw State University in spring 2018, and joined Dr. Mingon Kang's research lab. During his tenure as Graduate Research Assistant at Data X Lab, he made publications and received capstone project awards. His areas of interest includes Deep Learning, Machine Learning, Natural Language Processing, Computer Vision, and Android application development.